JOURNAL OF SOLID STATE CHEMISTRY 61, 8–39 (1986)

High-Resolution Electron Microscopic Study of Manganese Silicides $MnSi_{2-x}$

H. Q. YE

Institute of Metals Research, Academia Sinica, Shen-yang, Peoples' Republic of China

AND S. AMELINCKX*

Universiteit Antwerpen (RUCA) Groenenborgerlaan 171, 2020-Antwerp, Belgium

Received February 4, 1985

Several members of the family of Nowotny phases with compositions $MnSi_{2-x}$ are studied by means of electron diffraction and high-resolution electron microscopy. The diffraction patterns exhibit spacing as well as orientation "anomalies." From the corresponding high-resolution images it is concluded that the compounds exhibit a particular type of disorder. The spacing anomalies result from the fact that the manganese and silicon arrangements have different and to some extent independent periods along the c direction of the tetragonal structure. The orientation anomaly is due to the fact that the silicon helices can be shifted longitudinally along the c axis of the manganese sublattice. Dislocation-like arrangements of lattice fringes can consistently be explained by means of this model.

1. Introduction

High-resolution electron microscopy has recently contributed significantly to our understanding of "incommensurate" diffraction patterns. In particular, it has become possible to distinguish between patterns due to "pseudoincommensurate" structures, for which the incommensurate nature of the diffraction pattern has to be attributed to the presence of a regular mixture of commensurately spaced interfaces, and genuine incommensurate structures, such as deformation-modulated structures with a modulation wave vector, which varies continuously with temperature. It is the purpose of this paper to discuss the origin of the incommensurate nature of the diffraction pattern of some of the Nowotny phases or chimney-ladder structures (*1*). These phases have already been studied using electron diffraction and one-dimensional lattice fringes (*2*); a preliminary account of a recent high-resolution study of $MnSi_{2-x}$ ($x \simeq 0.25$) was given in Ref. (*3*). In particular, the high-resolution images will allow us to derive an unambiguous interpretation in terms of structural features of the moiré-like fringes observed at lower resolution.

2. Crystal Structures

The structure of the manganese silicides

* Also at SCK/CEN, 2400-MOL, Belgium.

0022-4596/86 $3.00

has been determined by Nowotny and coworkers (*1*). Atomic positions were published for four of these phases Mn_4Si_7 (*4*), $Mn_{11}Si_{19}$ (*5*), $Mn_{15}Si_{26}$ (*6*), and $Mn_{27}Si_{47}$ (*7*).

The building principle is the same for all of them, however. The transition metal atoms form a β-tin-like arrangement with a tetragonal subcell with lattice parameters $a = 0.552$ nm and $c_{Mn} = 0.437$ nm. The silicon atoms form a coupled helical arrangement with a period c_{Si} equal to approximately 4 times c_{Mn} and occupying interstices in the tetragonal manganese sublattice. The manganese atoms form the chimneys within which the silicon atoms are arranged in a "ladder." It is to be expected that the manganese arrangement will be slightly position-modulated as well with the same period (*2*).

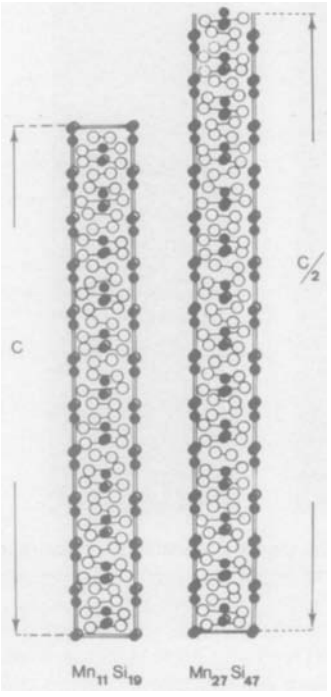

FIG. 1. Models for two Nowotny phases $Mn_{11}Si_{19}$ and $Mn_{27}Si_{47}$ as viewed along the [010] zone. Manganese atoms are represented as full dots; they form a body-centered tetragonal lattice. Silicon atoms are represented as open dots; they occupy interstices in the manganese sublattice (after Ref. (*1*)).

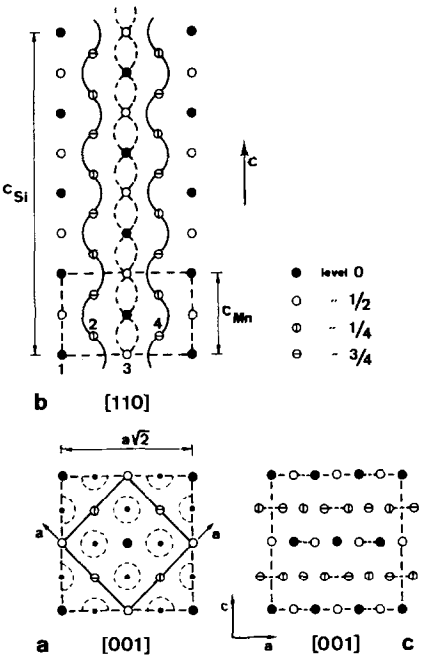

FIG. 2. Structure of the chimney ladder structures as related to the $TiSi_2$ structure. (a) The transition metal atoms are situated at four different levels; (b) the silicon atoms are situated on helices which project as the dotted circles in the [001] projection shown in (a); (c) in $TiSi_2$ the helices degenerate into planar zigzag configurations, parallel with the (110) planes, destroying the tetragonal symmetry; $TiSi_2$ is orthorhombic.

Models for two of these structures are represented in Fig. 1 (after (*1*)) and a more schematic representation is introduced in Fig. 2 emphasizing the relationship with the $TiSi_2$ structure. As we shall see the c parameter is the smallest common multiple of c_{Mn} and c_{Si}; for some of these phases the c parameter may become as large as 20 nm. We shall see also that in some phases c_{Mn} and c_{Si} may be incommensurate.

Three projections, respectively, along the [100], [110], and [120] zones of the structure of a typical phase $Mn_{15}Si_{26}$ are represented in Figs. 3A, B, and C [after (*6*)].

The large dots represent the projections of manganese columns whereas the small dots represent silicon columns. In the [110]

projection the Mn columns form a quasi-hexagonal arrangement; in the other projections the manganese columns form close pairs. The silicon columns form a wavy arrangement which is clearly the projection of the helical arrangement in space. In the [110] and in the [120] projections this leads to pronounced maxima in the electron density localized along lines perpendicular to the c axis and with a spacing equal to c_{Si}. These projections will be used as the input data for image simulation.

The structures of these compounds with general formula M_nSi_{2n-m} can also be related to the $TiSi_2$ structure. The transition metal atoms are arranged on 3^6 nets on (110) planes of the tetragonal subcell; these planes are stacked in the 1234 stacking sequence which occurs in $TiSi_2$ and which we have described above as the β-tin-like arrangement (Fig. 2).

Whereas in the tetragonal $MnSi_{2-x}$ structure the silicon atom positions are situated on helices projecting as circles along the [100] zone (Figs. 2a and b), these circles degenerate into planar zigzag arrangements in $TiSi_2$ (Fig. 2c) reducing the symmetry to orthorhombic.

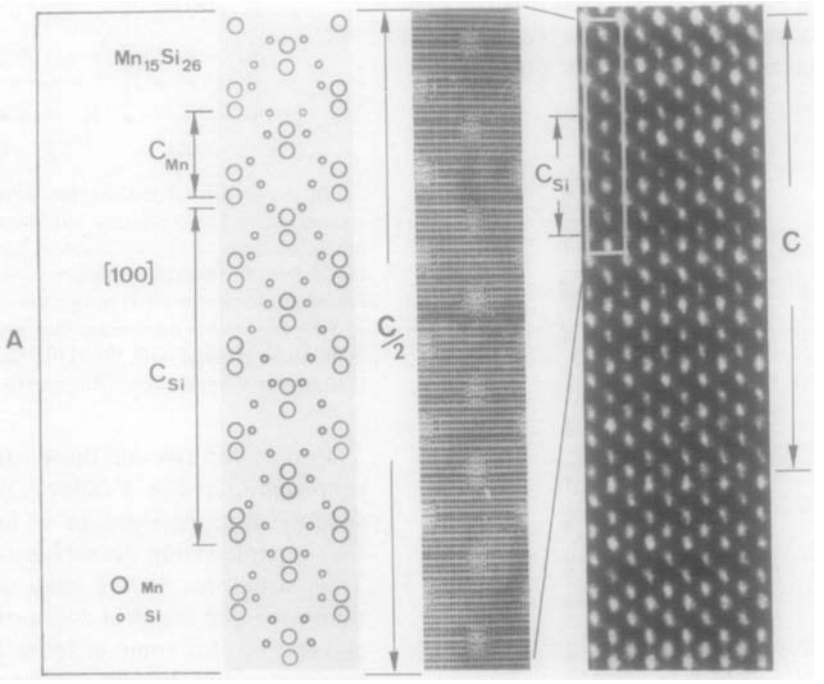

FIG. 3. (A) Comparison of the projected structure model, the computer-simulated image, and the experimental image of $Mn_{15}Si_{26}$ as viewed along [100] zone. The bright dots represent close pairs of manganese columns for $\Delta f = -97.5$ nm and $t = 5.5$ nm or $\Delta f = -150$ nm and $t = 16$ nm. (B) Comparison of the projected structure model, the computer-simulated image, and the experimental image of $Mn_{15}Si_{26}$ as viewed along the [110] zone. The bright dots represent single manganese columns ($\Delta f = -150$ nm, $t = 6$ nm). The bright bands occur where silicon and manganese columns coincide approximately. Their separation is very closely the pseudorepeat distance of the silicon arrangement. (C) Comparison of the projected structure model, the computer-simulated image, and the experimental image as viewed along the [$\bar{1}$20] zone. The elongated bright dots have to be associated with open channels in the structure ($\Delta f = -128.7$ nm; $t = 7.5$–10 nm). The bright bands occur where silicon and manganese columns roughly coincide; their separation is equal to the pseudoperiod of the silicon arrangement c_{Si}. The brightest dots correspond to open channels.

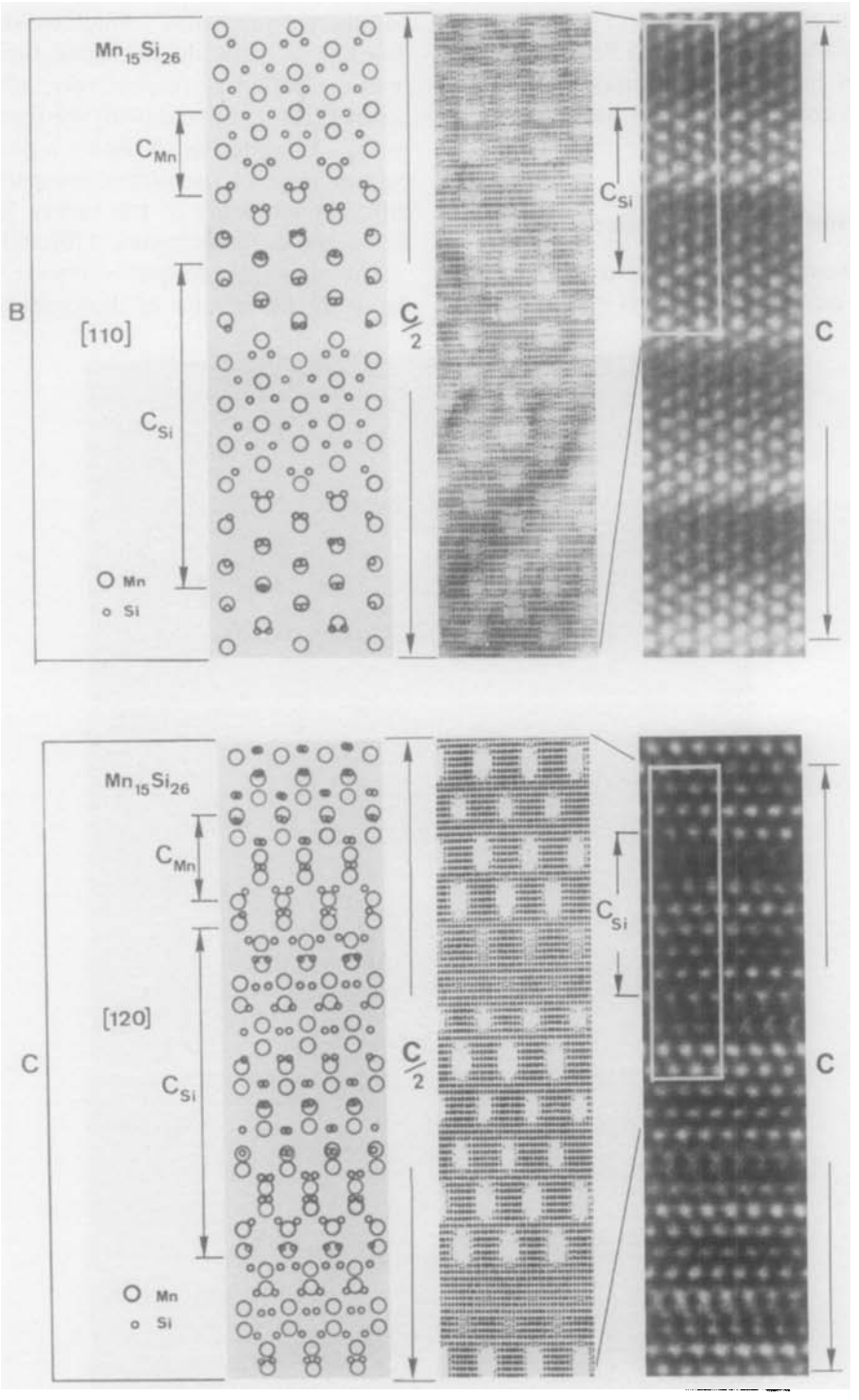

FIG. 3—*Continued.*

Chemical bonding in these materials was discussed by Jeitschko and Parthé (*8*); they noted in particular the importance of the electron concentration per transition metal atom.

3. Electron Diffraction Patterns

As already pointed out in earlier pages (*2*) the diffraction patterns exhibit a wide variety of "anomalies" which we shall now describe in some detail. Three typical diffraction patterns, respectively, along the zones [1$\bar{1}$0], [$\bar{1}$20] and [010] are reproduced in Fig. 4, while Fig. 5 shows a number of central rows of the diffraction patterns of different members of the family $MnSi_{2-x}$, along two different zones [110] and [120].

The most intense spots coincide with, or occur in the vicinity of those spots of the

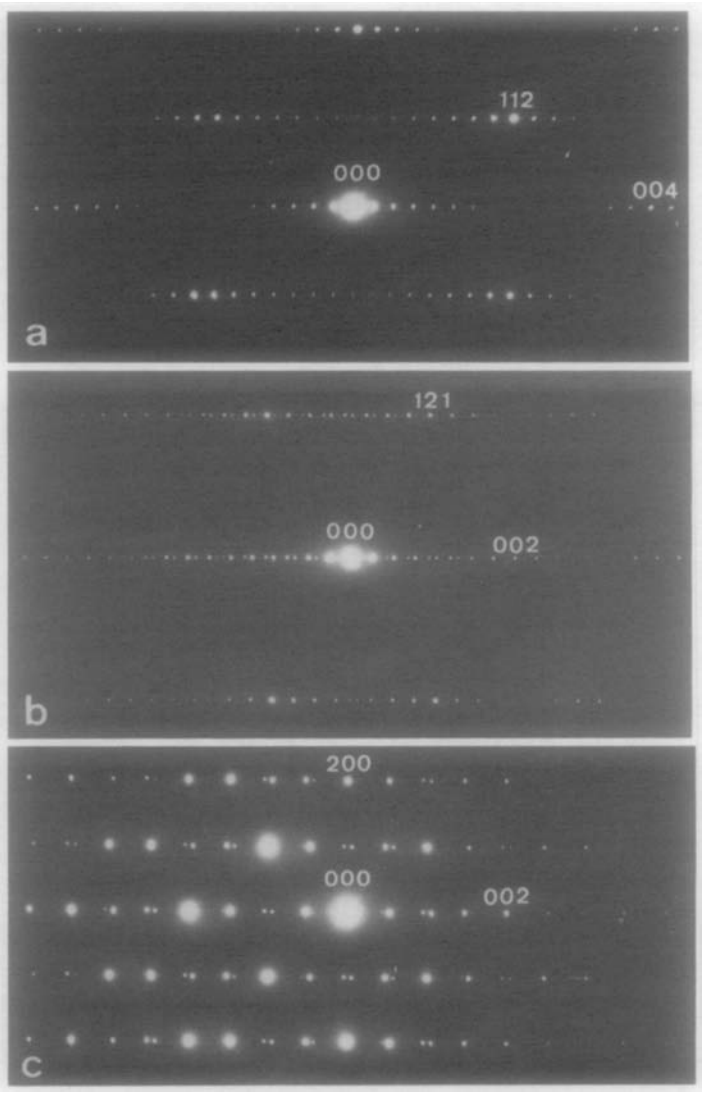

FIG. 4. Diffraction patterns of $MnSi_{2-x}$ taken along different zones: (a) [1$\bar{1}$0] zone; (b) [$\bar{1}$20] zone; (c) [010] zone.

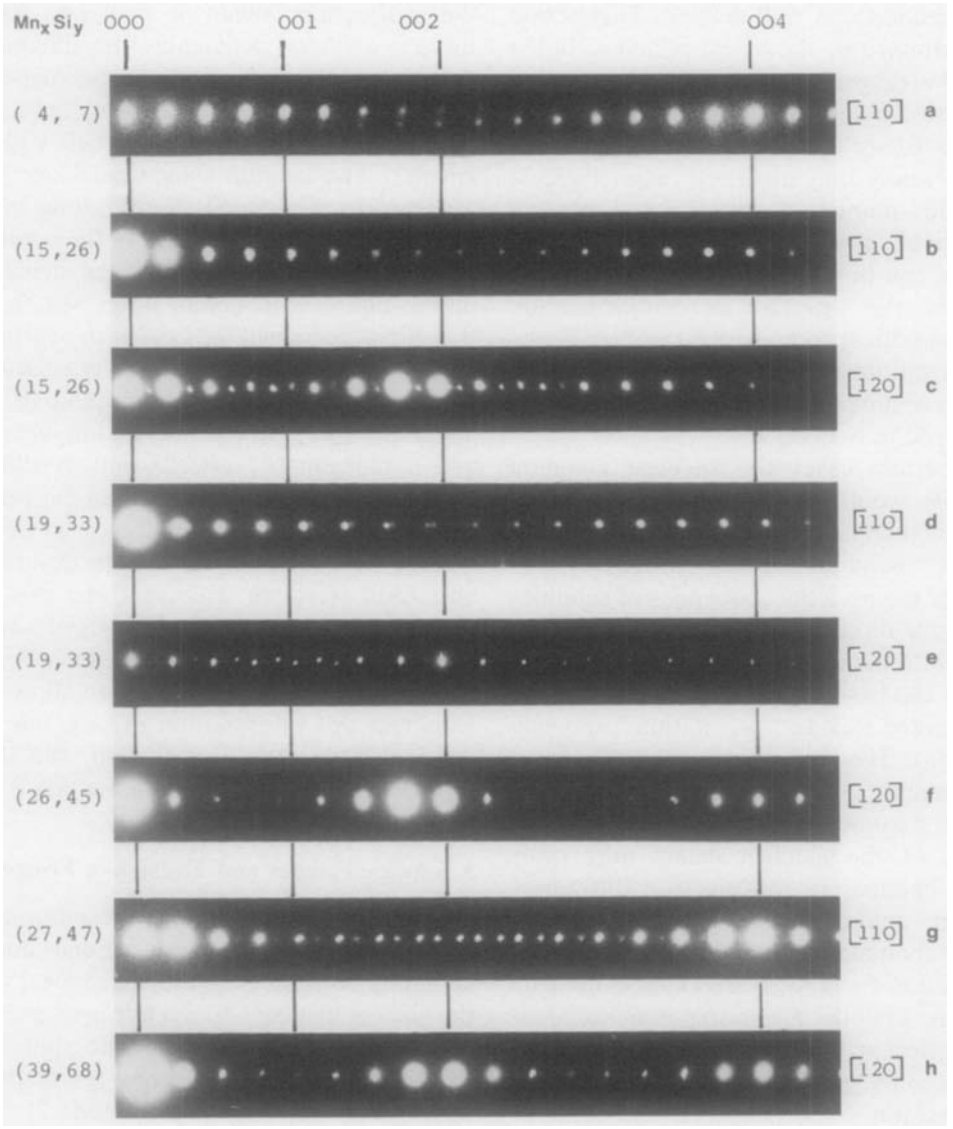

FIG. 5. Central [001] rows of the diffraction patterns of a number of compounds Mn_xSi_y along the [110] and the [120] zones. The values of x and y are indicated on the left. Commensurate as well as "incommensurate" diffraction patterns, exhibiting spacing and orientation anomalies are shown.

sequence which are due to the centered tetragonal sublattice of manganese atoms, i.e., 002, 004. With each of these "basic" spots a linear sequence containing up to 10 satellite spots is associated. As opposed to what happens in interface-modulated long-period superstructures these sequences of satellites are not "shifted" with respect to the basic spots (*2*). The spacing in direct space corresponding with the satellite spacing is only approximately equal to $4c_{Mn}$. From the large number of sharp satellites and their slow decrease in intensity with increasing order, i.e., with distance away from the "basic" spots, one can conclude that the lattice period giving rise to the sat-

ellite sequence is well defined. This period is determined by the repeat period c_{Si} of the helical arrangement of silicon atoms.

In most cases the sequences of satellites associated with different basic spots do not match where they meet (see, e.g., Figs. 5a or d). In a number of cases it is possible that a relatively small common multiple for c_{Mn} and c_{Si} can be found; it is then justified to describe the structure as commensurate. The theoretical composition can then be derived from the diffraction pattern provided certain assumptions are made. This will be discussed in Section 8.

In certain cases the smallest common multiple would become excessively large and it is then justified to consider the structure as "incommensurate." Moreover, in a number of cases the sequences of satellites may have directions which enclose a small angle with the direction of the rows of spots due to the basic manganese sublattice. We have called this an "orientation" anomaly (Fig. 5a). The structure is then no longer tetragonal.

Heat treatment of manganese silicides by means of the electron beam may bring about changes in the electron diffraction pattern; commensurate patterns may become incommensurate and may acquire an orientation anomaly. Such changes are usually irreversible. These experiments show that different diffraction patterns may be produced by specimens with the same bulk composition.

In the compound $MoGe_{2-x}$ which also has a chimney ladder structure it was found that specimens producing an "anomalous" diffraction pattern could be transformed by heat treatment into specimens presenting a "normal" diffraction pattern (*2*).

4. Structural Principle

For $MnSi_2$, i.e., for $m = 0$ one (001) layer contains one manganese and two silicon atoms, forming a pair at the same level along the c direction. When $m \neq 0$, i.e., when there is a silicon deficiency, the silicon atoms are still assumed to be arranged in pairs at the same level; however, the average number of pairs per unit cell will be smaller. The lacking silicon pairs are still assumed to be spaced evenly along the c direction since this is probably the configuration of minimum energy. In the structure of the phase with composition Mn_nSi_{2n-m} the silicon pairs will thus occur in m groups along the c axis, which can be regarded as pseudocells. Along the c direction of the superstructure one will thus find in *one* unit cell n manganese subcells and m silicon subcells. The c parameter is then the smallest common multiple of c_{Mn} and c_{Si}, i.e., $c = nc_{Mn} = nc_{Si}$. Assuming that the described structural principle is correct one can deduce the chemical composition from a measurement of c_{Mn}, c_{Si}, and c. A geometrical analysis of the diffraction pattern allows us to obtain this information; in fact, one reciprocal lattice row is sufficient. We shall discuss this in some detail in Section 8.

5. Lattice Fringes and Moiré-like Fringes

Observations at moderate resolution allow us to visualize the lattice fringes corresponding with the satellite sequences, i.e., the silicon spacing (*2*). Such fringes are obtained when successive satellite spots belonging to the same basic spot are made to interfere as shown in Fig. 6 (mode 2). The fringes are perpendicular to the satellite sequences, and their spacing corresponds with the silicon period (Fig. 7b). Spots belonging to two *different* satellite sequences, such as those surrounded in Fig. 6 (mode 1), which occur in the part of the diffraction pattern where two satellite sequences meet or overlap, can also be used to make an image. Such images consist of broad, often wavy fringes which are the more widely spaced the closer the collected spots. These fringes are perpendicular to the segment $\bar{\Delta}\bar{g}$

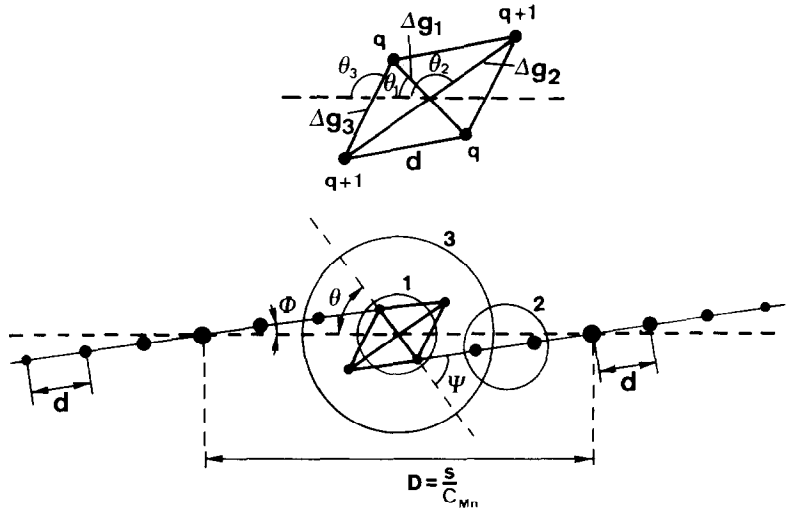

FIG. 6. Schematic representation of one row of spots of the diffraction pattern exhibiting an orientation and a spacing anomaly. Three different imaging modes are indicated by circles enclosing the beams which are used. The meaning of a number of notations is illustrated as well.

connecting the two interfering satellite spots (Fig. 7c) and this distance is inversely proportional to $|\bar{\Delta}\bar{g}|$. This has been verified experimentally by means of dark-field images made in such spot pairs. The direction and spacing Λ of these fringes is found to vary over the area of the specimen suggesting that $\bar{\Delta}\bar{g}$ changes locally. It should be noted that the direction of $\bar{\Delta}\bar{g}$ is very sensitive to small changes in the direction of the satellite sequences. These moiré-like fringes provide in fact a map of the vector $\bar{\Delta}\bar{g}$, and thus of the spacing and orientation anomalies.

Finally, one can collect several spots belonging to two interleaving satellite sequences (Fig. 6, mode 3). The image now exhibits both types of fringes simultaneously (Fig. 7a) and it is clear that the two sets of fringes enclose an angle which varies over the specimen area. Whereas the narrowly spaced "silicon" fringes are practically straight, the more widely spaced moiré-like fringes are wavy and intersect the silicon fringes under the angle $\Psi = \theta + \phi$ (Fig. 7a).

The relation between θ, Ψ, and ϕ can be found from Fig. 6. One has $\Lambda = 1/|\bar{\Delta}g|$

$$(\Delta g)^2 = 4q^2d^2 + D^2 - 4qdD\cos\phi$$

$$\operatorname{tg}\theta = \frac{2qd\sin\phi}{|D - 2qd\cos\phi|} \qquad (1)$$

$$\Psi = \theta + \phi$$

using the notation indicated in Fig. 6; q is the number of satellites on one side of the basic spot.

From Eq. (1), noting that $1/c_{Si} = d\cos\phi$ and $c_{Si} = (q + \varepsilon)c_{Mn}$; $D = s/c_{Mn}$ one finds

$$\operatorname{tg}\theta = \frac{2q\sin\phi/c_{Si}\cos\phi}{(s/c_{Mn}) - (2q\cos\phi/c_{Si}\cos\phi)}$$

$$\operatorname{tg}\theta = \operatorname{tg}\phi/[(s/2q)(q + \varepsilon) - 1].$$

For $s = 2$, this becomes

$$\operatorname{tg}\theta = (q/\varepsilon)\operatorname{tg}\phi. \qquad (2)$$

In direct space the generation of an "orientation anomaly" can be visualized as in the simple model of Fig. 8.

A systematic shift upward over εc_A was given to the pattern of dots with respect to the pattern of bars leading to a shear over an angle ϕ of the dot pattern. This can alter-

natively be described as a translation downward over qC_A. The coincidence pattern is then sheared over an angle θ. It is quite clear that tg $\phi = \varepsilon C_A/a$ and tg $\theta = qC_A/a$ and thus tg $\theta = -(q/\varepsilon)$tg ϕ where the minus sign expresses the opposite sense of ϕ and θ.

This relation is clearly equivalent to Eqs. (1) and (2) obtained from reciprocal space considerations.

Since

$$c_{Si} = (n/m)c_{Mn} = (q + \varepsilon)c_{Mn} \quad (2')$$

one can rewrite Eq. (2) as

$$\text{tg } \theta = -q \text{ tg } \phi/[(n/m) - q]. \quad (3)$$

It should be noted that in Mn_4Si_7, $\varepsilon = 0$ and thus $\theta = 90°$ provided $\phi \neq 0$. In $Mn_{15}Si_{26}$: $q = 3$; $\varepsilon = \frac{3}{4}$ and tg $\theta = 4$ tg ϕ (using $\bar{\Delta}\bar{g}_1$ in Fig. 6)); using $\bar{\Delta}\bar{g}_2$ in Fig. 6 one has $q = 4$;

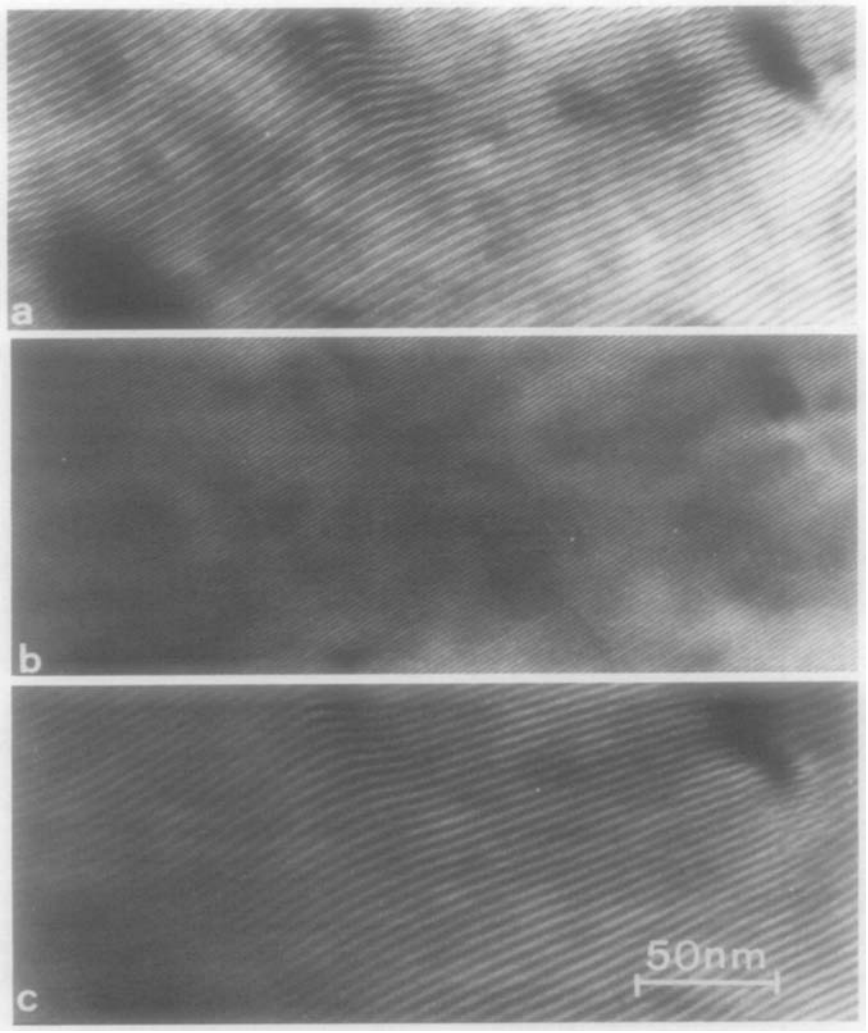

FIG. 7. One-dimensional lattice fringes in manganese silicides obtained from the same area by using different imaging modes. (a) Mode 3: moiré-like fringes superposed on silicon fringes. The moiré fringes map the spatial variation of $\bar{\Delta}\bar{g}$. (b) Mode 2: the fringes represent the period of the silicon arrangement. (c) Mode 1: only moiré-like fringes are produced.

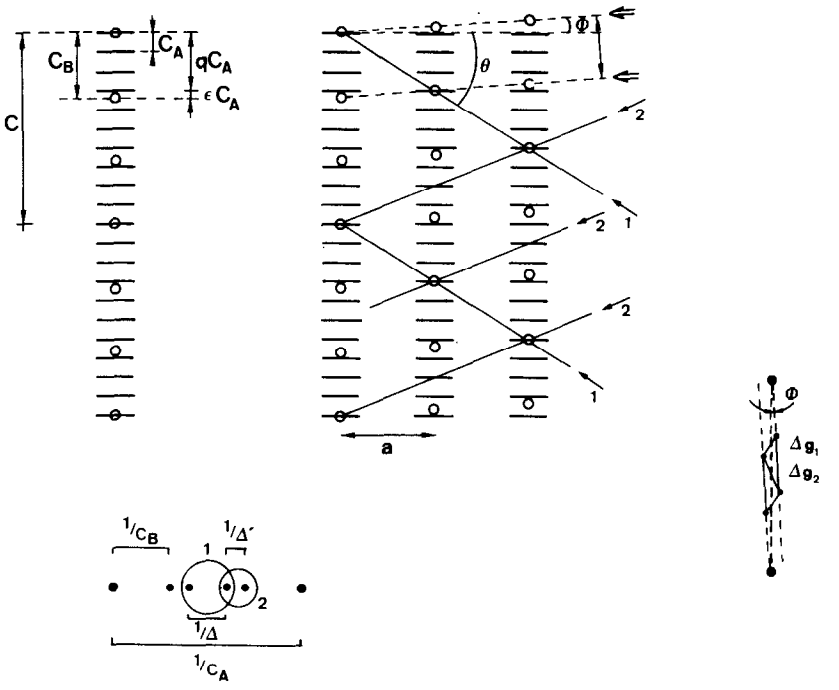

FIG. 8. Schematic illustrating that a small systematic shift of the dot pattern over an angle ϕ with respect to the line pattern, leads to a much larger change in orientation of the coincidence lines along 1 and 2. The relevant diffraction vectors $\bar{\Delta}\bar{g}_1$ and $\bar{\Delta}\bar{g}_2$ are shown in the correct relation with the line-and-dot pattern.

$\varepsilon = -\frac{1}{4}$, tg $\theta = 16$ tg ϕ. The angular amplification factor can thus be considerable.

If is, of course, possible to select other spot pairs such as the qth satellite in one sequence and the $(q + 1)$th satellite in the other sequence and then obtain moiré-like fringes with a wave vector such as $\bar{\Delta}\bar{g}_3$ in Fig. 6.

It is possible finally to collect the four spots forming a parallelogram in Fig. 6. One thus obtains the silicon fringes and superposed on this a crossed grid of moiré-like fringes with wave vectors $\bar{\Delta}\bar{g}_1$, $\bar{\Delta}\bar{g}_2$, and $\bar{\Delta}\bar{g}_3$. The characteristics of such fringes can be calculated by the use of formula (1) provided the correct value of q is taken for $\bar{\Delta}\bar{g}_1$, $q = 3$; for $\bar{\Delta}\bar{g}_2$, $q = 4$. For $\bar{\Delta}\bar{g}_3$ the formula has to be adapted slightly.

Similar sets of superposed lattice and moiré-like fringes have been observed in $Au_{3+}Zn$ (*9*), where the latter fringes reveal the true period.

6. High-Resolution Images

6.1. Methods

High-resolution images were obtained for a number of members of the $MnSi_{2-x}$ family, using different imaging modes and viewing along different zones: [110], [120], and [100] (Figs. 3A, B, and C, respectively).

Use was made of a 200-kV high-resolution electron microscope with a c_s value of 1.2 mm. The computer-simulated images were obtained along the same zones but only for the phase on which the most detailed structural information is available, i.e., $Mn_{15}Si_{26}$ (*4*), of which the structure is

represented along three different zones in Fig. 3. Use was made of the well-known multislice method (*10*).

The following values of the different parameters were adopted: electron wavelength 2.51×10^{-3} nm (corresponding to 200 kV); $c_s = 1.2$ mm; incident beam divergence 0.75×10^{-3} rad; defocus due to the chromatic aberration 7 nm; objective aperture radius 7 nm^{-1}. The slice thickness was different in the three cases: [100] zone—0.55 nm; [110] zone—0.39 nm; and [120] zone—0.62 nm.

We shall first comment on the images of the simplest "commensurate" materials and discuss the corresponding simulated images.

6.2. [110] Zone

The left side of Fig. 3B is a schematic view of the structure of $Mn_{15}Si_{26}$ as seen along the [110] zone. This is compared with the corresponding simulated image represented at the same scale and in the correct spatial relationship with the model, and computed using the parameters given above. The defocus value and the thickness are, respectively, $\Delta f = -150$ nm and $t = 6$ nm. Only half of the unit cell is shown and compared with the indicated area of the observed image. It is clear that the prominently bright dots occur at positions along which manganese and silicon atoms project along the same columns and thus give rise to sharp peaks in projected potential. When the distribution of projected potentials is more uniform, less pronounced bright dots occur at the positions of the manganese columns and the broad darker fringes result. The modulation period corresponds with the quasiperiod of the overlap pattern of the manganese and the silicon arrangements which we have called c_{Si}, since it is directly related to the larger period of the silicon arrangement.

Figure 9 shows the bright- and dark-field images of the compound $Mn_{27}Si_{47}$ viewed along the [110] zone which is the most informative one. The dark-field image (Fig. 9b) was taken by including four basic spots forming a lozenge as well as their associated satellite spots. This is the minimum information required to image the manganese sublattice. The configuration of bright dots in this zone should be compared with the scheme of Fig. 3B; this suggests that the bright dots image the manganese sublattice since their configuration and scale in Fig. 9 are the same as those of the dots representing the manganese columns in Fig. 3B.

Although Fig. 3 represents a different member of the family, namely $Mn_{15}Si_{26}$, this comparison is valid since the manganese sublattice is very nearly the same for all members.

Figure 9a shows the corresponding bright-field image made by collecting the direct beam and two sets of basic reflections around it, together with their satellites; here again the bright dots have the correct geometry to represent the manganese sublattice as can be seen by comparing with Fig. 3B.

In both images the brightness of the dots is modulated with a period c_{Si} which is equal to the period of the silicon helices. Referring to the schematic projection of Fig. 3B along the same zone, this can easily be understood since also the distribution of atom columns is modulated with the same period. At one level silicon and manganese atoms form mixed columns and hence the columns are relatively widely spaced; at a level differing by $\frac{1}{2}c_{Si}$ the columns are more uniformly spaced and contain either Mn or Si and are thus much less densely populated.

Also the computer-generated images exhibit this periodic modulation of the dot brightness with period c_{Si}. In Fig. 9b we have marked the repeat period of the manganese sublattice c_{Mn} deduced from the bright-dot pattern and that of the silicon sublattice c_{Si} derived from the dark fringes.

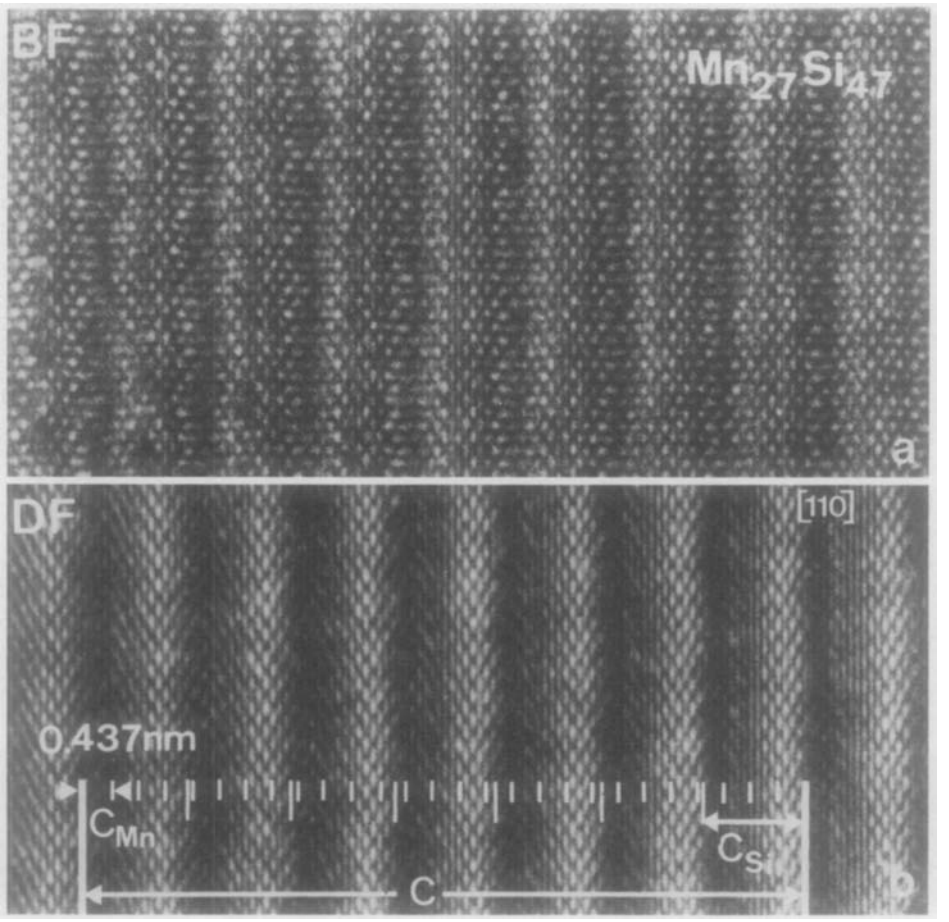

FIG. 9. Bright- and dark-field images of the compound $Mn_{27}Si_{47}$ viewed along the [110] zone. (a) Bright-field image—BF; (b) dark-field image—DF. The silicon and the manganese spacings are indicated on the dark-field image, as well as the c parameters.

The smallest common multiple c is indicated as well. The corresponding theoretical composition is thus $Mn_{27}Si_{47}$ (see Section 8).

From Fig. 3B it is clear that in a row along the c direction, three or, at most, four columns are sufficiently well defined, because the projections of Mn and Si columns are sufficiently close to be imaged as a single somewhat broadened bright dot; this is consistent with the experimental images.

The high-resolution image of $Mn_{19}Si_{33}$ along the same zone is reproduced in Fig. 10; we have again indicated separately the repeat periods for the silicon and for the manganese sublattices.

Finally, one of the simplest members of the family, namely Mn_4Si_7, is represented in Fig. 11, with separate indications of the manganese and of the silicon periods: $c_{Si} = 4c_{Mn} = c = 1.78$ nm.

6.3. *[120] Zone*

Figure 3C reproduces the [120] view of the compound $Mn_{15}Si_{26}$, whereas a more extensive area is presented in Fig. 12. The modulations of the spot brightness are also present in this view although in a somewhat

less pronounced manner than in the [110] view. The image can be compared with the schematic representation of Fig. 3C and with the computed image along the same zone. A [$\bar{1}$20] view of the $Mn_{19}Si_{33}$ compound is reproduced in Fig. 13.

The [120] zone schematic view of Fig. 3C is drawn at the same scale and in the correct spatial relationship with the simulated images made along the same zone of the phase $Mn_{15}Si_{26}$ (with $\Delta f = -128.7$ nm and a thickness $t = 7.5$–10 nm). This in turn is compared with the observed image of which the area within the rectangle corresponds with the simulated image. The intensity modulation of the bright dots is quite obvious and one notes again that the prominently bright dots occur at places where silicon and manganese atoms project along the same column and as a consequence leave open channels. The bright dots are slightly elongated in the c direction and have to be associated with the channels in the manganese framework which occur in these parts of the structure where the projections of manganese and silicon atoms coincide.

The c period of the manganese sublattice c_{Mn} in the [110] and [120] images is much smaller (~4 times) than that of the silicon arrangement and it contains moreover four rows of manganese atom columns per period. As a result the quasicoincidences of the atom columns which give rise to the pronounced intensity modulations in the image occur with a pseudoperiod c_{Si} primarily determined by the silicon arrangement.

6.4. [100] Zone

A [100] view of the compound $Mn_{15}Si_{26}$ is reproduced in Fig. 3A. In this zone the configuration of the bright dots is the same in scale and orientation as that of the pairs of

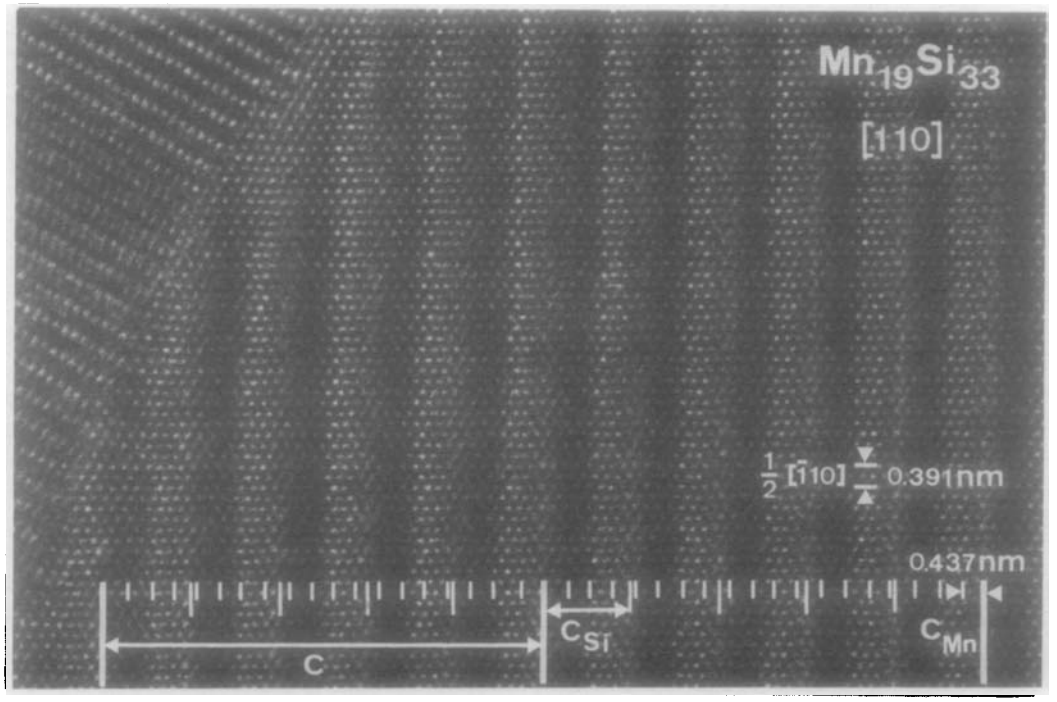

FIG. 10. High-resolution bright-field images of $Mn_{19}Si_{33}$ along the [110] zone. The repeat periods of the manganese and silicon arrangements have been indicated separately.

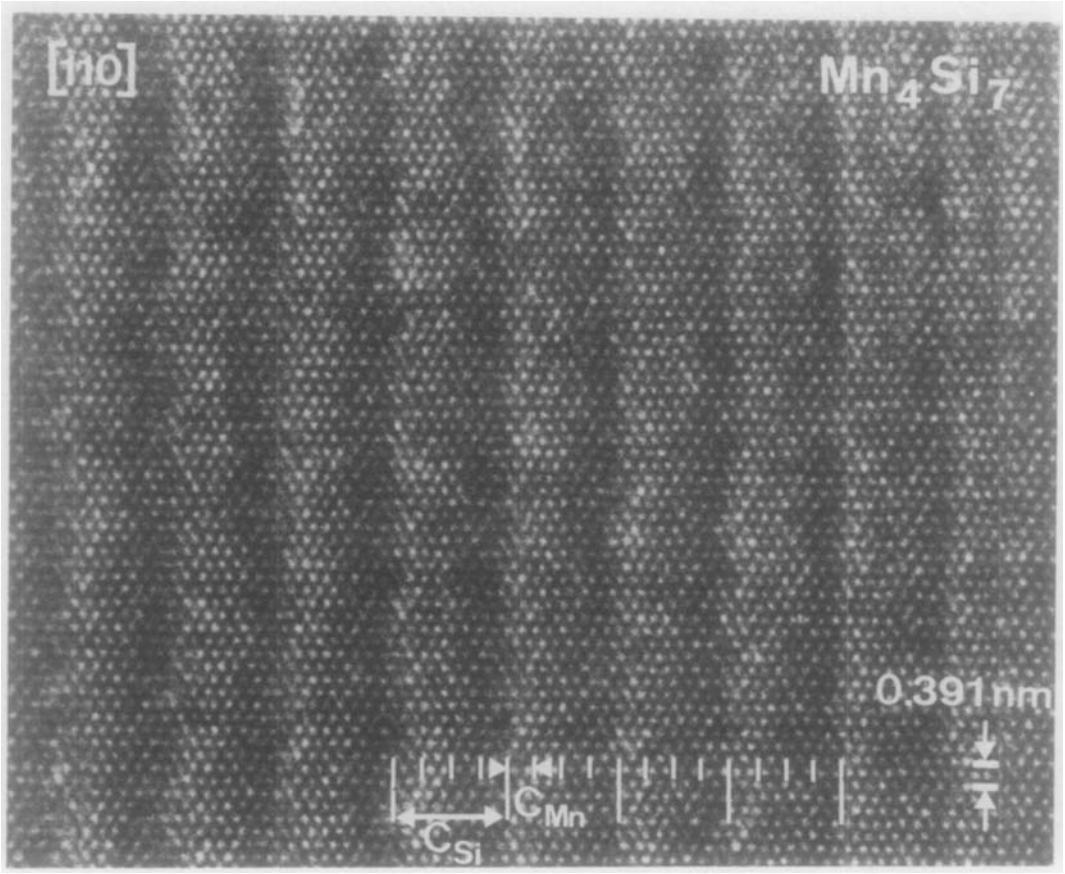

FIG. 11. High-resolution bright-field image of the simplest member of the family Mn_4Si_7 along the [110] zone. The repeat periods of the manganese and silicon arrangements have been indicated.

manganese columns suggesting that each bright dot represents a pair of manganese columns. However, this configuration is also the same as that of the channels in the structure and simulated images are required to decide between these two possibilities.

A comparison of the simulated ($\Delta f \simeq -128.7$ nm; $t = 5.5$ nm) and the observed ($\Delta f \simeq -100$ nm) images in Fig. 3A represented at the same scale and in their correct spatial relationship allows us to conclude that the prominently bright dots have to be associated with pairs of manganese columns, rather than with channels in the structure.

The brightness modulation is hardly visible, but it is nevertheless present. It becomes evident especially at lower magnification. The dark lines between the rows of bright dots alternate in intensity in Fig. 14; this is particularly visible when looking at grazing incidence along the modulation. Also the schematic view of the silicon columns in Fig. 3A exhibits to a good approximation a double periodicity; two silicon configurations alternate along the c axis.

Figure 14a shows the [100] zone of another phase than $Mn_{15}Si_{26}$ and at a somewhat smaller magnification; the modulation can now better be observed and hence it has been possible to indicate separately the spacings c_{Si} and c_{Mn}; it is found that this phase must be rather complicated because

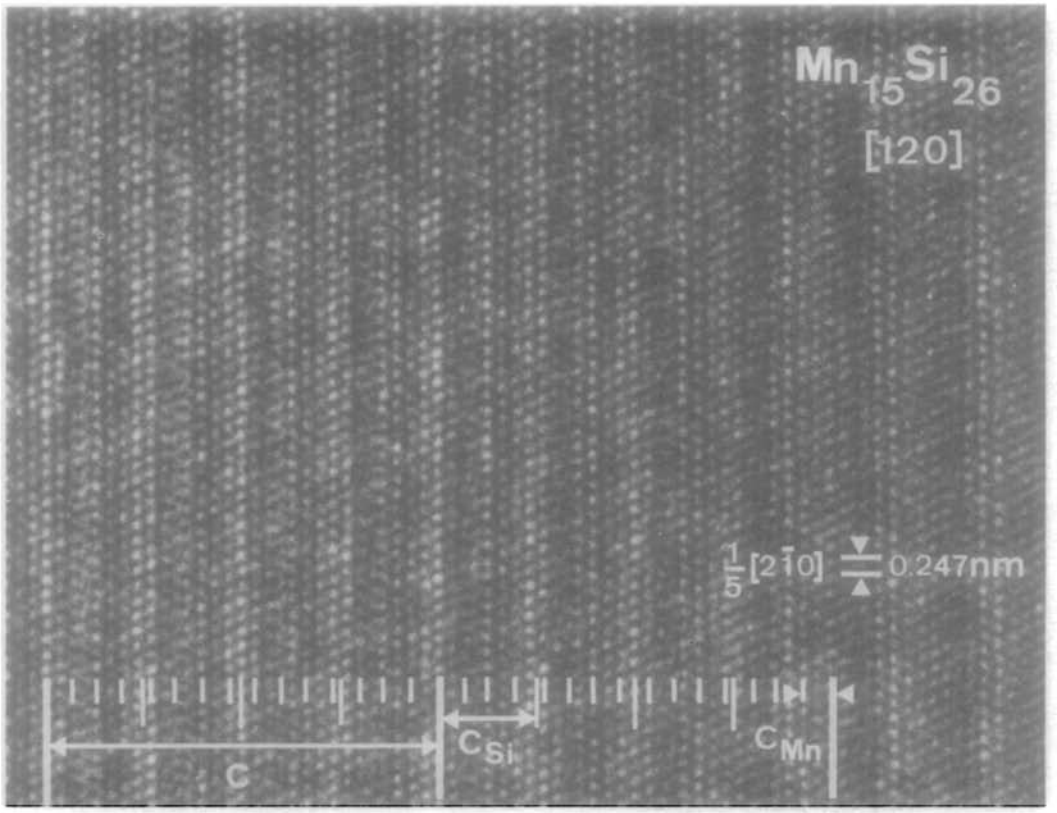

FIG. 12. Bright-field image of $Mn_{15}Si_{26}$ along the [120] zone.

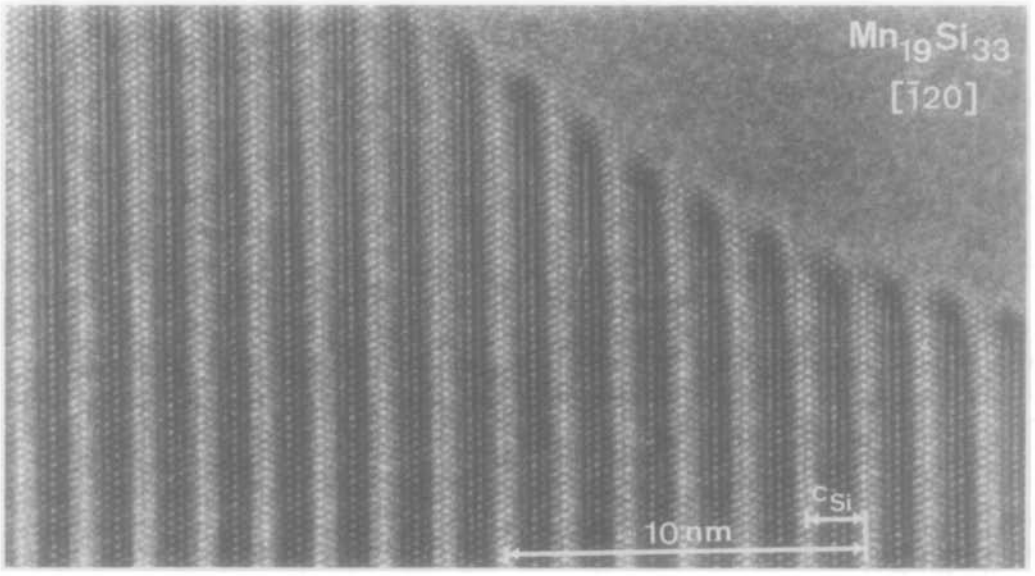

FIG. 13. High-resolution image along the [$\bar{1}$20] zone of $Mn_{19}Si_{33}$.

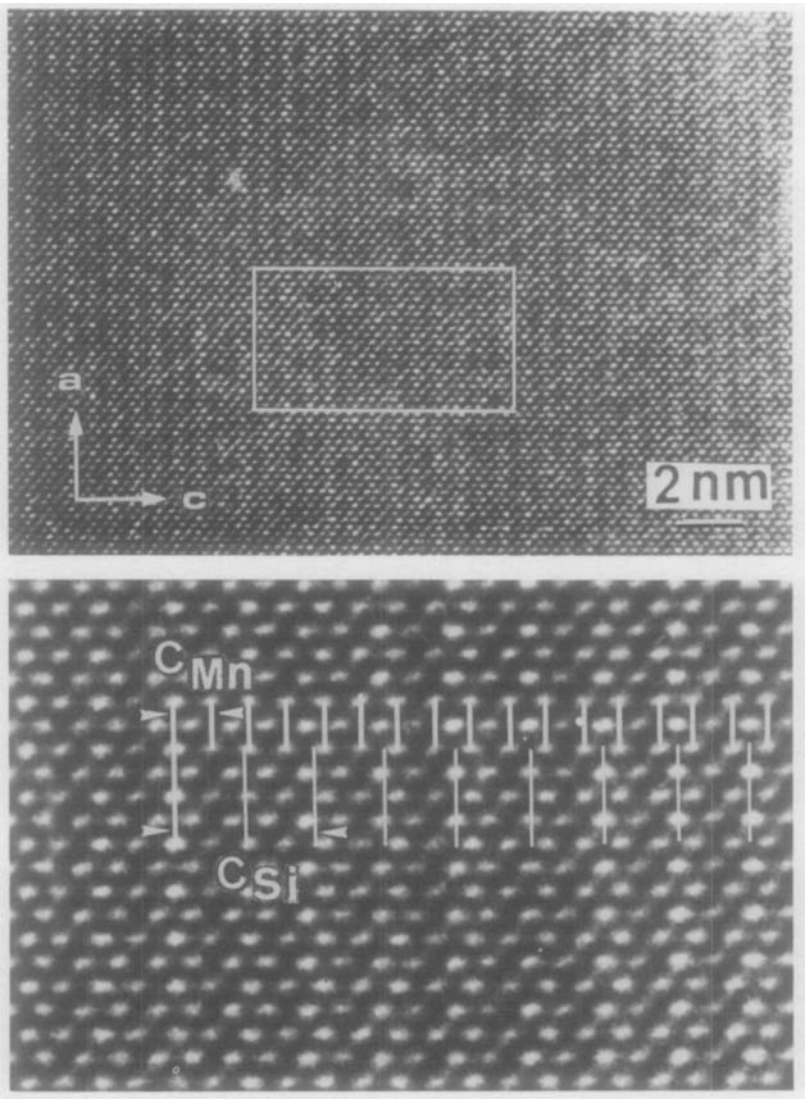

FIG. 14. (a) [100] View of $MnSi_{2-x}$ exhibiting clearly the modulation of the intensity of bright dots. In this case the distance c_{Si} contains two pseudoperiods of the silicon arrangement, i.e., two bands of the modulation pattern. The periods c_{Mn} and c_{Si} have been indicated separately in (b). The c parameter must be larger in this case since coincidence between the two "verniers" is not achieved within the considered rectangle.

no coincidence is found within a reasonable distance for the "vernier" formed by the two spacings. It should be noted that in this projection the distance c_{Si} corresponds to *two* interfringe distances as a result of the particular atomic arrangement along this zone, as is evident from Fig. 3A.

7. Orientation Anomalies

We shall now discuss a few examples of images made from parts of the specimen which give rise to diffraction patterns exhibiting a visible orientation anomaly. Figures 15a and b are such images viewed

along the [$\bar{1}$20] zone. One clearly observes an orientation difference between the rows of bright dots, which we have attributed to the manganese sublattice, and the broad modulations which we have related to the silicon period. The angle between these two sets of fringes is equal to the angle ϕ deduced from the diffraction pattern (Fig. 6).

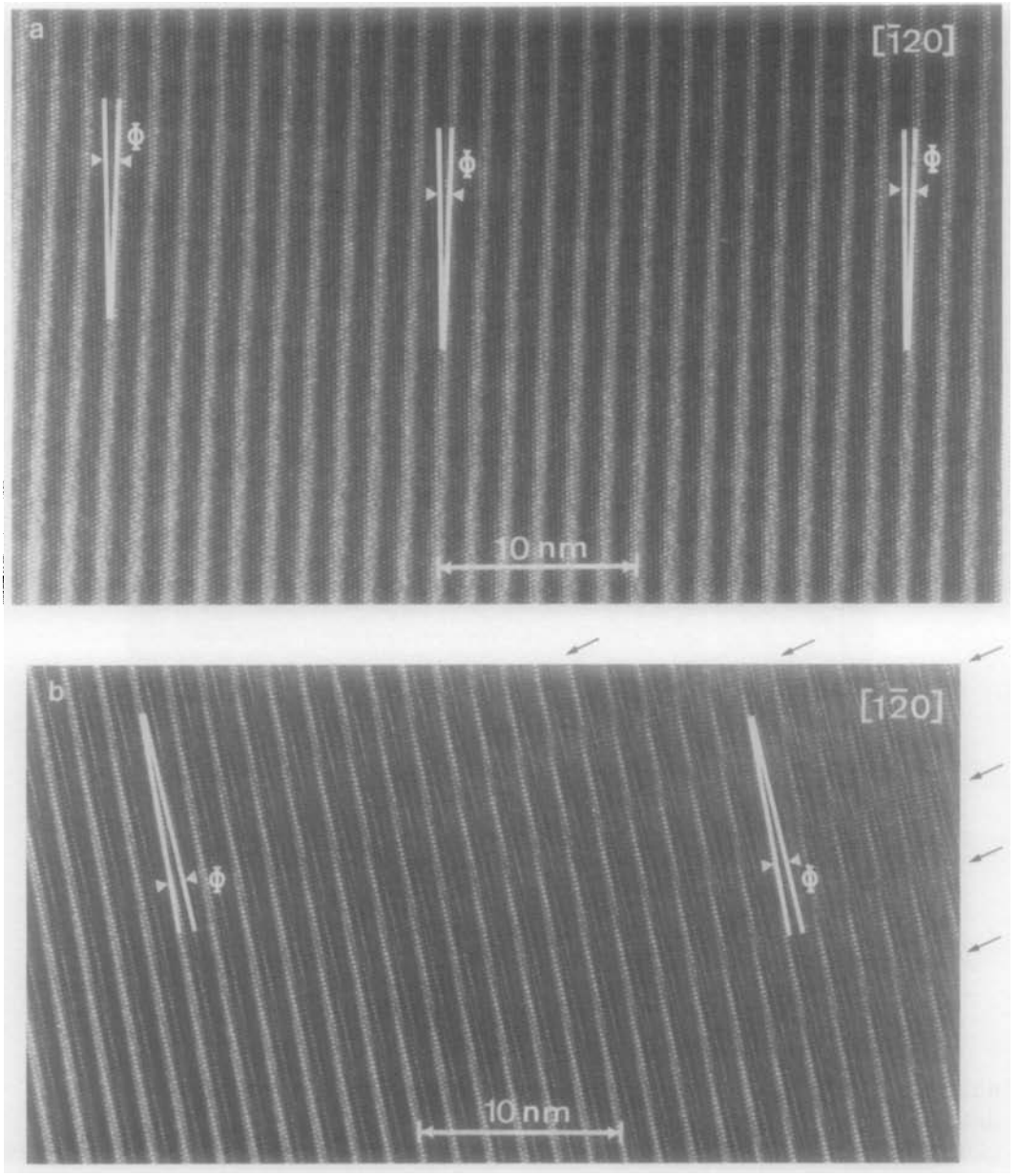

FIG. 15. (a) High-resolution image along the [$\bar{1}$20] zone of a region exhibiting an orientation anomaly in the diffraction pattern. The angle ϕ between the "silicon" fringes and the "manganese" fringes is indicated. (b) The angle ϕ is larger in this case. Note the intensity modulation of the silicon fringes, revealing the broad moiré-like fringes along the arrows.

The direction of the fringes, which we assume to be the average orientation of the planes of "equal phase" of the modulation due to the silicon arrangement, is thus not perpendicular to the c axis. This suggests that the helical configurations of silicon atoms may be shifted along the c axis in adjacent rows of manganese unit cells or possibly stepwise every nth row of manganese unit cells. If this shift is systematic and gradual, as represented schematically in Fig. 8, the planes of equal "phase" of silicon helices are still plane but no longer perpendicular to the c axis of the manganese sublattice. The shift of the Si helices may change nonsystematically along the specimen giving rise to spatially varying orientation anomalies and hence to moiré-like fringes of arbitrary shape, as described in Section 5 (see also (*3*)). The angle Ψ of these moiré-like fringes with the "silicon" fringes is related to the angle ϕ of the silicon fringes with the manganese fringes by the relations (1) and (2).

8. Image Simulation of Orientation Anomaly

We have also attempted to simulate the high-resolution image of a crystal area containing an orientation anomaly such as in Fig. 15. We are then faced with the problem of first proposing a detailed model, which implies the determination of a large number of atomic positions in a suitably chosen unit cell, in view of the application of the method of periodic continuation. This unit cell has to be sufficiently large in order to represent a realistic situation, but still small enough to be tractable by the computer. Taking these limitations into account we have chosen to make the calculation for the simplest among the phases: Mn_4Si_7 as viewed along the [120] zone. Since we have no observations of orientation anomalies in a specimen which can with certainty be attributed to the Mn_4Si_7 phase and since Mn_4Si_7 is in fact an exceptional case as far as orientation anomalies is concerned, no detailed comparison is possible but at least we can make our interpretation plausible.

The atomic positions in a specimen containing an orientation anomaly are not available from X-Ray diffraction results. A reasonable first approximation for such data can be obtained by shifting the silicon helices along a rigid manganese "chimney" over a repeat distance of the manganese sublattice. Of course restrictions are imposed by the fact that the interatomic distances should have realistic values and furthermore the building principle of these compounds must be obeyed as closely as possible.

Empirically it is found that the shortest Mn–Si distance in $Mn_{15}Si_{26}$ is 0.23 nm; furthermore, also the Si–Si separation along the chimneys must be conserved as closely as possible. By drawing arcs of circles around the manganese atoms at different levels along the chimney one can select small triangular areas, formed by circular segments, and which enclose allowed positions for the projections of silicon columns. This was done in Fig. 16a where such areas have been indicated for one single chimney and for different levels. As a result the projections of silicon columns are limited to positions roughly projecting along the dotted square in Fig. 16a. The actual allowed positions were chosen along a square which rounded corners, shown in Fig. 16b.

There are four such chimneys in one unit cell. The idealized positions in space are situated on four cylindrical surfaces, which can be approximated by the square prisms I, II, III, and IV as in the spatial view of Fig. 16c. The successive positions along a helix in one manganese subcell are connected by line segments. It should be noted that as required the silicon atoms clearly systematically avoid the manganese atoms which are present at the corners and in the

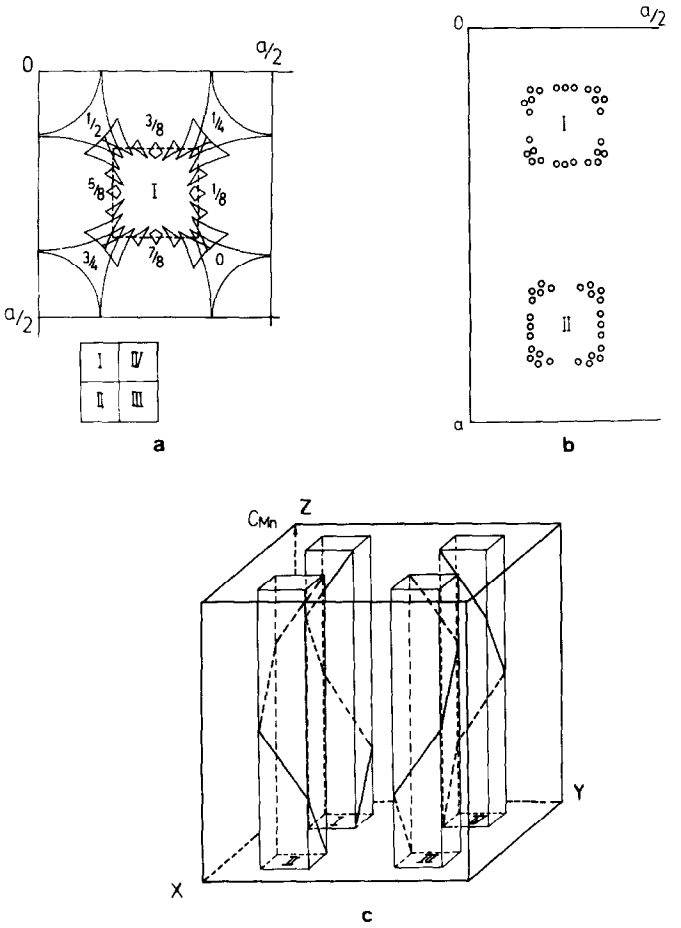

FIG. 16. (a) Schematic representation of one of the "chimneys" in the $MnSi_{2-x}$ structure. The arcs of circles have radii equal to the shortest distances Mn–Si and Si–Si. The small triangular areas are "allowed" regions for the projection of silicon sites. (b) The projections of Si sites are shown as dots. (c) Spatial arrangement of the helical-like configuration of silicon atoms in the four chimneys of the manganese sublattice.

side faces of the tetragonal prism in eccentric positions.

The building principles of these compounds now require that if one pair of silicon atoms occupies positions on the prisms I and III the silicon pair in the next level has to occupy positions on the prisms II and IV. The arrangements in II and III and in I and IV are related by symmetry.

In the selected model a Mn_4Si_7-like structure was assumed to contain four manganese subcells of the type represented in Fig. 16 and 14 pairs of silicon atoms.

In order to simulate the structure responsible for the orientation anomaly the silicon helices in successive manganese chimneys were shifted along the [001] directions over a distance of about 0.02 nm which is somewhat more than 1% of the c_{Si} distance and which leads to a uniform "shear" of the silicon arrangement over an angle of about 4.6° which is within the observed range as

deduced from the diffraction pattern and from the high-resolution images. In each level the silicon atoms were assumed to occupy the most likely positions, as deduced above, after the shift was applied. This small shift in the positive sense of the helices relative to the manganese matrix results in a much larger shift in the opposite sense of the overlap configuration of the manganese and silicon arrangements. This is a consequence of the well-known "vernier" effect illustrated schematically in Fig. 8. Consequently, the traces of the bands of "coincidence" columns which are imaged as widely spaced diffuse fringes undergo an orientation change which is much larger than the "shear angle" of the silicon arrangement; in the particular case considered it becomes of the order of 30°. This is demonstrated schematically in Fig. 17 where the manganese sublattice, represented as full dots, has been kept undeformed, whereas the arrangement of open dots, representing silicon atoms, has been shifted downward along the vertical direction when going from left to right while the arrangement was after every shift adjusted to represent the equilibrium positions deduced above. The orientation of the traces of the bands of coincidence (the moiré-like fringes) can be observed by looking along the single arrows; they are sloping upward when going from left to right.

Half of the area shown in Fig. 17 was used as the artificial unit cell for the image simulation of which the results are shown in Fig. 18. It is clear that the diffuse band is sloping upward from left to right over an angle of about 30° in accordance with the model. This calculation, although only representing approximately the real situation and in particular exaggerating the angular

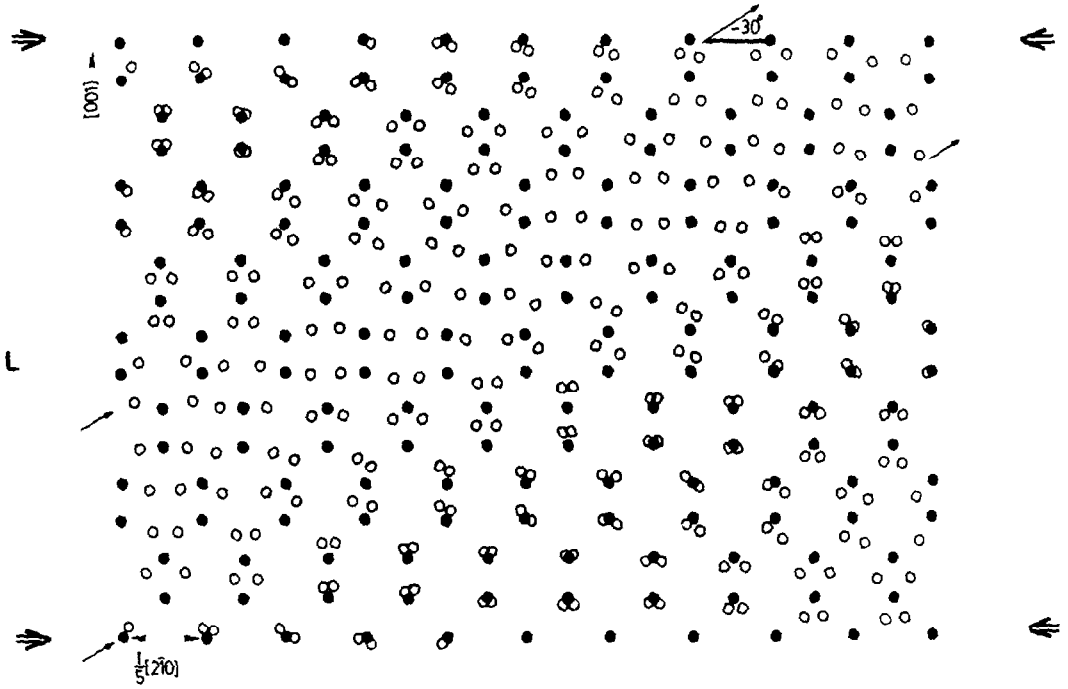

FIG. 17. Projected atom positions in a crystal area of the Mn_4Si_7 type whereby the silicon helices have suffered a small systematic shift in successive vertical "chimneys." The manganese sublattice remained undeformed. The "coincidence" sites are situated on an inclined band enclosing an angle of 30° with the horizontal direction.

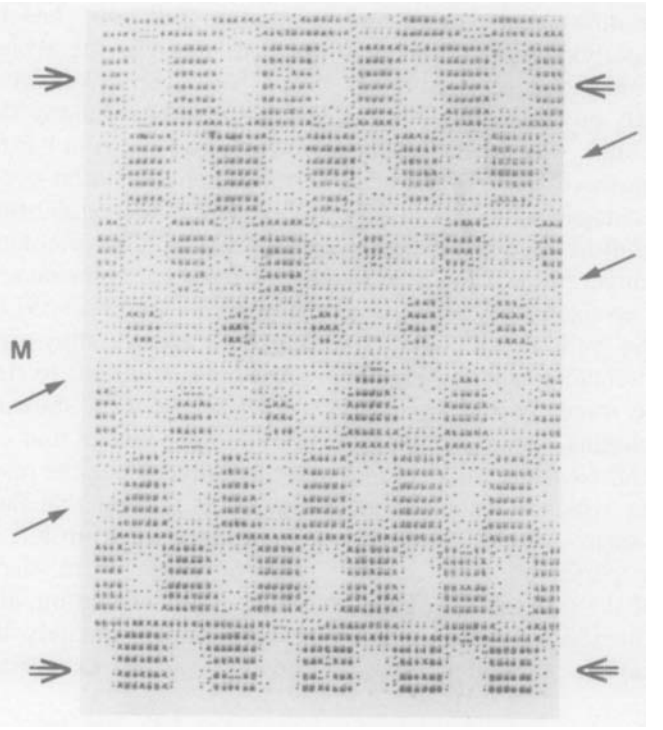

FIG. 18. Image simulation of the model of Fig. 17 demonstrating that the small shift of the silicon helices leads to a much larger change in orientation of the moiré-like fringes which are formed along the coincidence band of Fig. 17 and are indicated by single arrows. The double arrows indicate the silicon fringes.

differences makes it plausible that the orientation anomaly should be attributed to systematic shifts of the helical arrangement of silicon atoms along the "chimney" in the manganese sublattice. The "silicon fringes" also related to the coincidence columns have changed very little in orientation. They are indicated by the double arrows in Figs. 17 and 18. The area covered is somewhat too small to see clearly the periodic brightness variation of the bright dots along the silicon fringes; but some indication of this can nevertheless be noticed. The moiré-like fringes are indicated by single arrows in Figs. 17 and 18.

At low resolution one can observe simultaneously the silicon fringes and the moiré-like fringes (Fig. 7a); the manganese sublattice is not revealed. The dark moiré-like fringes are in fact imaged as the intensity minima in the silicon fringes which they intersect.

The high-resolution images on the other hand reveal the silicon fringes and the manganese arrangements, but the moiré-like fringes usually are too broad to be observed. Also, since many beams contribute to the image, they are not well defined since several formation modes operate simultaneously. In Fig. 15b it is nevertheless possible to observe weak broad bands formed by the locus of the intensity maxima and minima in the silicon fringes (look along the arrows!). They enclose an angle of about 75° with the manganese rows; the silicon rows enclose an angle of about 8–10° with the manganese rows. A detailed interpretation is not possible in this particular case

since we do not know the values of m and n.

9. Relationship between composition, diffraction pattern, and images

Assuming the model described in Section 3 to be valid it is possible to establish a simple relationship between the ideal composition Mn_nSi_{2n-m}, the diffraction pattern and the high-resolution image. We shall only consider the case where no orientation anomaly is present; the central row of the diffraction pattern is then as represented schematically in Fig. 19 along the [120] and [110] zones. Figure 5 shows actual examples; the indices indicated on the photographs refer to the Mn sublattice.

Let the spacing anomaly be represented by p/m' expressed as a fraction of c_{Si}. We first consider the [120] zone. Let there be q satellites associated with the origin between 000 and 001. If the distance between two basic spots, i.e., $(2qm' + 2m' - p)/2$ is integral $m = m'$ and $n = [2(q + 1)m - p]/2$; if not $m = 2m'$ and $n = 2(q + 1)m - 2p$.

In the [110] zone there are extinctions and the relation is slightly different; if $(2qm' + 2m' - p)/4$ is integral, $m = m'$ and $n = [2(q + 1)m - p]/4$. Knowing n and m the lattice parameter c follows from $c = nc_{Mn} = mc_{Si}$.

It should be noted that the intensities of the spots due to the Mn sublattice are very sensitive to small orientation differences; the 002 and 004 spots are therefore not always the strongest in the sequence. It is therefore necessary to determine unambiguously the positions of the 002 and 004 spots when indexing the diffraction pattern.

The high-resolution images allow us to determine directly the numbers m and n, by looking for a coincidence of the "vernier" formed by the scales of the c_{Si} and of the c_{Mn} spacings, deduced as mentioned above and indicated on some of the images, such as Figs. 9 and 12. If m widely spaced fringe spacings match with n rows of bright dots the composition is Mn_nSi_{2n-m}.

Using the methods outlined here we have determined the composition of seven different compounds for which we have obtained commensurate diffraction patterns as well as high-resolution images; their characteristics are represented in Table I. For four of the six compounds X-ray studies had been performed previously; good correspondance is found for the c parameters determined from the images with those known from X rays.

In the absence of an orientation anomaly there is also a simple relation between the spacing Δ of the moiré-like fringes and the composition. Let us assume that the two central spots form the moiré-fringes (mode 1 in Fig. 6). From Fig. 19 one can conclude

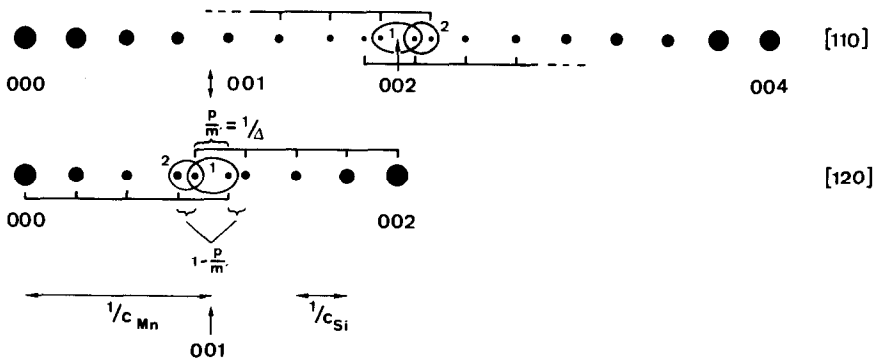

FIG. 19. Schematic representation of spacing anomalies along the [110] and [120] zone patterns.

TABLE I

OBSERVED COMMENSURATE STRUCTURES Mn_nSi_{2n-m}

Chemical formula Mn_xSi_y	Atom ratio x/y	Orientation	Electron diffraction pattern (spacing anomaly)		Image $mc_{Si} = nc_{Mn}$		C parameter	
					m	n	Image	X-Ray
Mn_4Si_7	1.75	110	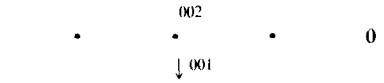	0	1	4	17.79	17.46
Mn_7Si_{12}	1.714	120	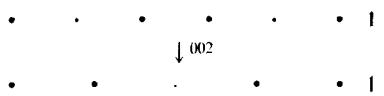	1	7	2		
$Mn_{15}Si_{26}$	1.733	110	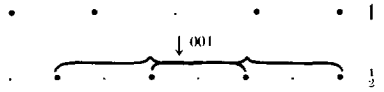	1	4	15	65.38	65.55
		120	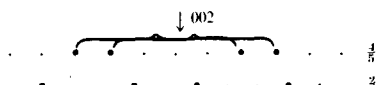	$\frac{1}{2}$	4	15	65.75	65.55
$Mn_{19}Si_{33}$	1.737	110	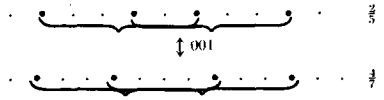	$\frac{4}{5}$	5	19		
		120	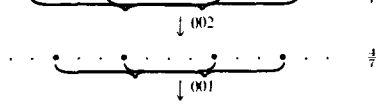	$\frac{2}{5}$	5	19		
$Mn_{26}Si_{45}$	1.731	120	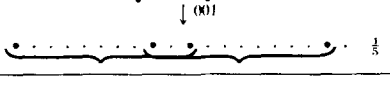	$\frac{3}{7}$	7	26	113.8	113.36
$Mn_{27}Si_{47}$	1.741	110	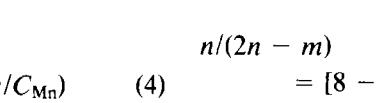	$\frac{4}{7}$	7	27	117.56	117.94
$Mn_{39}Si_{68}$	1.744	120	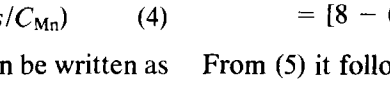	$\frac{1}{5}$	10	39		

that

$$(2q/c_{Si}) - (1/\Delta) = (s/C_{Mn}) \qquad (4)$$

and since $mc_{Si} = nc_{Mn}$ this can be written as

$$(1/\Delta) = [2q - s(n/m)](1/c_{Si}), \qquad (5)$$

where $q = 4$ and $s = 2$ for the [120] zone and $q = 8$ and $s = 4$ for the [110] zone. This relation shows that Δ goes to infinity if $n = 4m$. This is consistent with the fact that there is no "spacing anomaly" for Mn_4Si_7. In $Mn_{19}Si_{33}$ one finds (for the [120] zone) that $\Delta = \frac{5}{2}c_{Si}$; in $Mn_{15}Si_{26}$, $\Delta = 2c_{Si}$ and finally in $Mn_{27}Si_{47}$ one has $\Delta = \frac{7}{2}c_{Si}$. The relation (5) between Δ and c_{Si} is illustrated by means of several examples in Fig. 20. It is clear that by measuring the ratio Δ/c_{Si} one can derive the ratio n/m from relation (5), i.e., for the [120] zone:

$$n/m = 4 - (c_{Si}/2\Delta)$$

and

$$n/(2n - m) = [8 - (c_{Si}/\Delta)]/[14 - 2(c_{Si}/\Delta)]. \qquad (6)$$

From (5) it follows further that

$$\Delta = [1/(2qm - sn)]c. \qquad (7)$$

For the [120] zone this expression becomes

$$\Delta = [1/(8m - 2n)]c. \qquad (8)$$

For all components studied in detail $8m - 2n = 2$ except for Mn_4Si_7 which does not produce moiré-like fringes ($\Delta = \infty$). The moiré-like fringes thus have a spacing $\Delta = \frac{1}{2}c$ which is simply related to the c parameter; they provide a map of the c spacing also in cases where an orientation anomaly is present.

In such cases where the angle θ is small the relation $\Delta = \frac{1}{2}c$ is still valid with a good approximation; in general it becomes $\Delta = \frac{1}{2}c \cos\theta$. When using the eccentric pair of

spots, mode 2 in Fig. 19, one obtains a moiré spacing Δ' given by $1/\Delta' = 1/c_{Si} - 1/\Delta$.

Using the formula (6) we can derive the local composition for the compounds of which the moiré-like fringes are reproduced in Figs. 7a and 20. The spacing of these fringes can easily be measured in units of c_{Si}, in areas where the two sets of fringes are approximately parallel, i.e., where there is no orientation anomaly.

For the part of Fig. 7a where the two sets of fringes are parallel one finds $\Delta = 2c_{Si}$ and hence the composition is $Mn_{15}Si_{26}$.

In the right part of Fig. 20a the moiré spacing Δ is alternatively 3 and 4, leading to an average value of $3.5c_{Si}$. Using formula (7) this leads to the composition $Mn_{27}Si_{47}$; in the top left part one has $\Delta = 3c_{Si}$ leading to a composition $Mn_{23}Si_{40}$ · (y/x = 1.7391).

In Fig. 20b the moiré spacing is approximately 10 times the silicon spacing; it is not well defined since the moiré fringes are broad and ragged; the composition corresponding with $\Delta = 10c_{Si}$ is $Mn_{79}Si_{138}$ (x/y = 1.7468). In Fig. 20d finally $\Delta = 12c_{Si}$ and the composition $Mn_{95}Si_{166}$ (y/x = 1.7473).

In Fig. 20c the moiré fringes enclose a large angle with the silicon fringes and the simple analysis leading to formula (7) is no longer justified.

From Fig. 6 it is clear that a small rotation of the sequence of satellites in the clockwise sense results in a rotation of $\bar{\Delta}\bar{g}$ in the opposite sense, assuming that c_{Si} remains unchanged. This behavior is illustrated in Fig. 20a where the directions of the silicon fringes are indicated by means of black lines, seen to rotate in the opposite sense of the moiré fringes.

Small rotations of the satellite sequences away from the parallel orientation (i.e., ϕ = 0) result in an increase of $\bar{\Delta}\bar{g}$, i.e., in a decrease of the fringe spacing Δ. This behavior is illustrated in Fig. 20e where the spacing of the moiré fringes is indicated for the parallel ($\phi = \psi = 0$) orientation and after rotation over a small angle ($\Psi \neq 0$).

In Fig. 20f the orientation of the moiré fringes changes over a larger angle, and it is quite obvious that their spacing decreases correspondingly; it is also evident that the silicon fringes, of which the orientation is indicated by black lines, rotate in the opposite sense of the moiré fringes, of which the orientation is indicated by white lines.

9. Insertion Defects

The combination of high-resolution images, electron diffraction, and computer simulation has made it possible to understand the origin of the anomalies observed in a number of electron diffraction patterns and which suggest some deviations from the ideal structure as determined by X-ray analysis of the compounds of the type Mn_nSi_{2n-m} with $m \ll n$.

It turns out that the helical arrangement of silicon atoms in neighboring columns of the Mn sublattice may be shifted one relative to the other in the c direction. This can be understood if the interaction between neighboring helices is considered to be weak as compared to the interaction with the manganese sublattice. It is then possible that the helices in neighboring chimneys, or in regularly spaced "chimneys," are shifted over c_{Mn} along the c axis or over any other among the symmetry translations of the Mn sublattice. Such a translation brings the manganese sublattice into coincidence but shifts the helices over a translation which is not a symmetry translation for the silicon arrangement. If such shifts occur in a systematic way the average direction of the planes of equal phase are no longer perpendicular to the c axis.

The form of disorder considered here may also give rise to the dislocation-like configurations observed in some specimens (Fig. 21). A dislocation-like configuration (such a defect could perhaps be called a

sublattice dislocation since only the silicon lattice is dislocated) can formally be generated by removing a single half plane (half row in projection) of silicon atoms in the lower part of the diagram of Fig. 22 followed by a slight rearrangement of the helices by longitudinal shifts in the c direction, i.e., in the chimneys. This small shift is directed to the right in the lower left part and to the left in the lower right part. The manganese sublattice remains undisturbed during the operation. Although the geometry resembles that of a dislocation the defect so formed is not a dislocation; in particular, the *supplementary* silicon half plane is localized where the dislocation-like configuration presents a *lacking* half fringe and, moreover, the manganese sublattice remains undislocated.

Although no image calculation could be performed because of the very large number of atoms to be taken into account, we can confidently conclude that the configuration represented in Fig. 22 would give rise

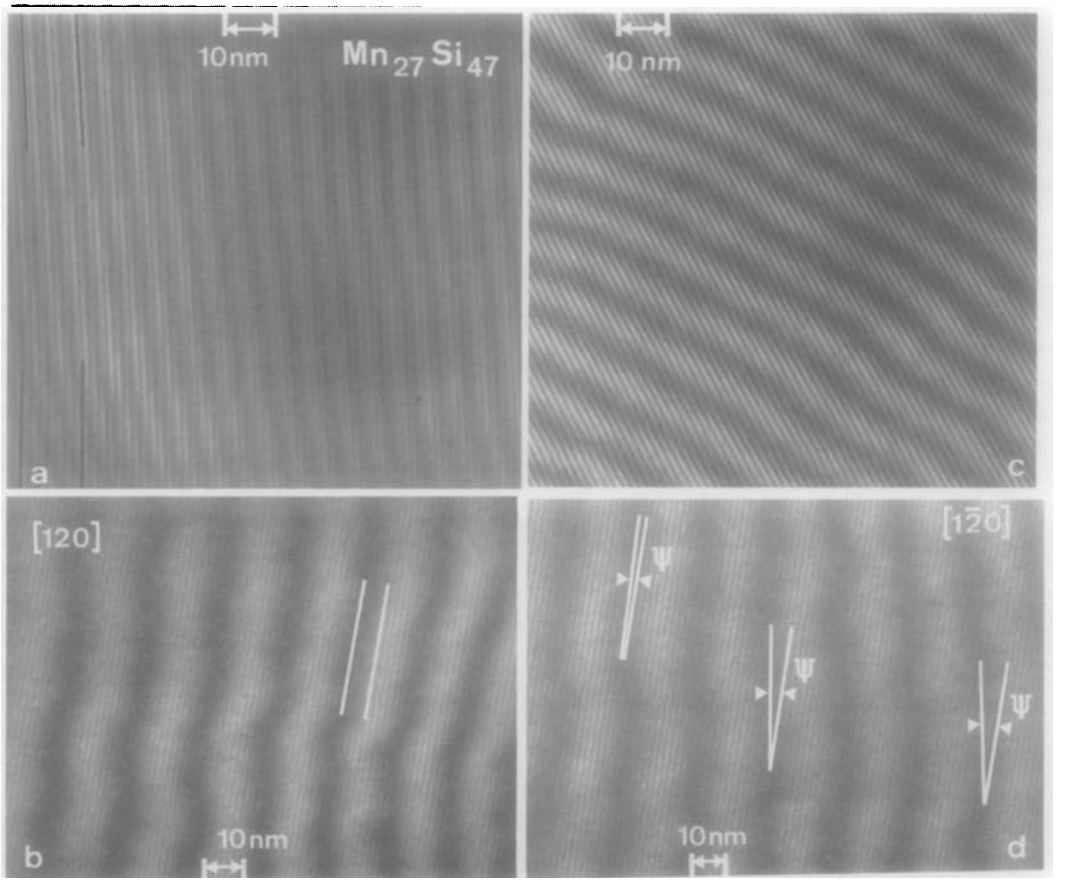

FIG. 20. (a–d) Four examples of moiré-like fringes superposed on "silicon" fringes. The angle Ψ enclosed between the two types of fringes is different in the four cases, and variable over the area. Also the spacing of the moiré-like fringes is different and somewhat variable. (e) The moiré-like fringes change orientation; note that the spacing decreases as they rotate away from the parallel orientation. (f) The moiré-like fringes change orientation over a larger angle; note the change in orientation of the silicon fringes in the opposite sense as well as the change in spacing of the moiré-like fringes.

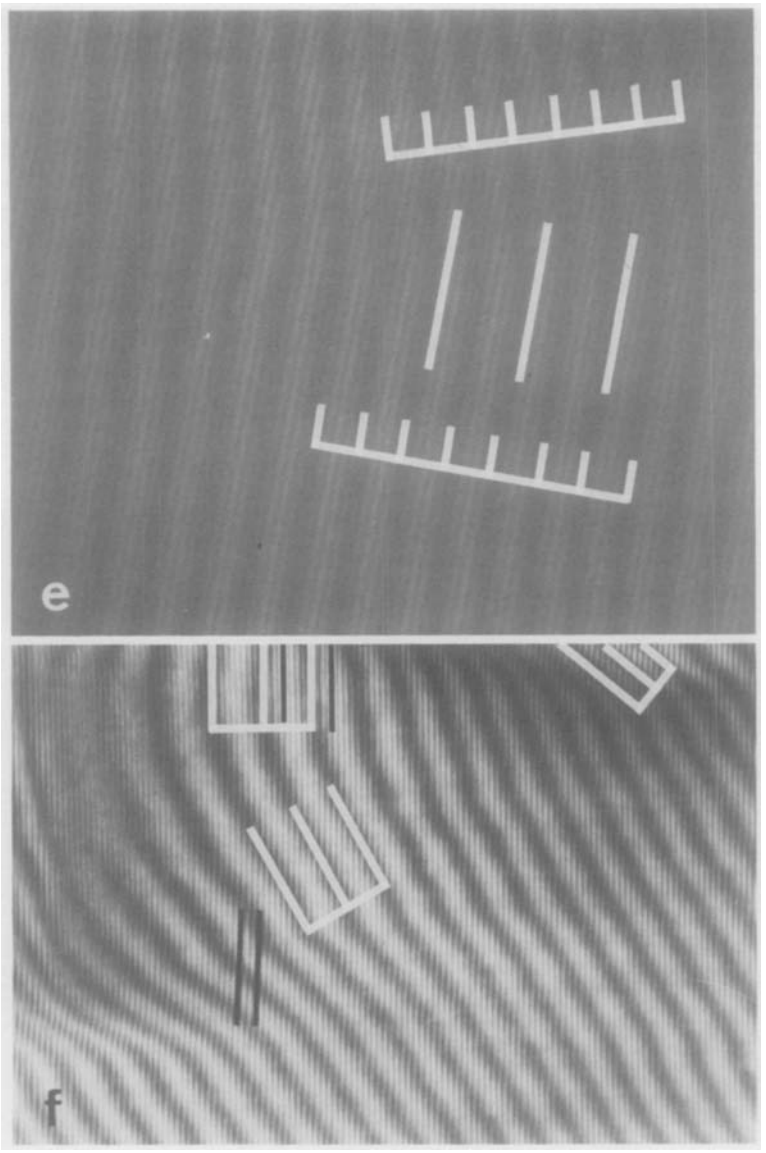

FIG. 20—*Continued.*

to an image such as the one of Fig. 21. This conviction is based on the results of the calculations described in Section 6.1 which clearly shows that the bright "silicon fringes" image near coincidence patterns between the two sublattices whereas the dark fringes correspond to noncoincidence regions. The image of the defect is highly magnified and broadened as compared to the atomic image of an ordinary dislocation. This is somewhat similar to the Moiré image of a dislocation revealed by the superposition of a perfect foil and a foil containing a dislocation, at low resolution. In fact the present dislocation images are comparable to such moiré images since they

result from the coincidence pattern of a perfect lattice (the manganese sublattice) and an interpenetrating dislocated one (the silicon sublattice).

Such "dislocation-like" configurations have also been observed at moderate resolution, revealing the silicon fringes only (Figs. 21a and b, inset). The weakness of the strain contrast in the vicinity of such defects shows that they are not dislocations; on the other hand this is consistent with our interpretation in terms of the insertion defects suggested here.

10. Relation between Moiré-like Fringes and High-Resolution Images

Figure 23a is an exceptionally informative high-resolution image in that it exhibits simultaneously all different types of fringes, as well as a "dislocation" in the silicon fringes. The viewing zone is [120]. At the edges of the specimen the resolution is sufficient to determine the composition. One finds very closely $n/m = q + \varepsilon = 3.5$, i.e., from Eq. (2′) the composition is Mn_7Si_{12} (Fig. 23b).

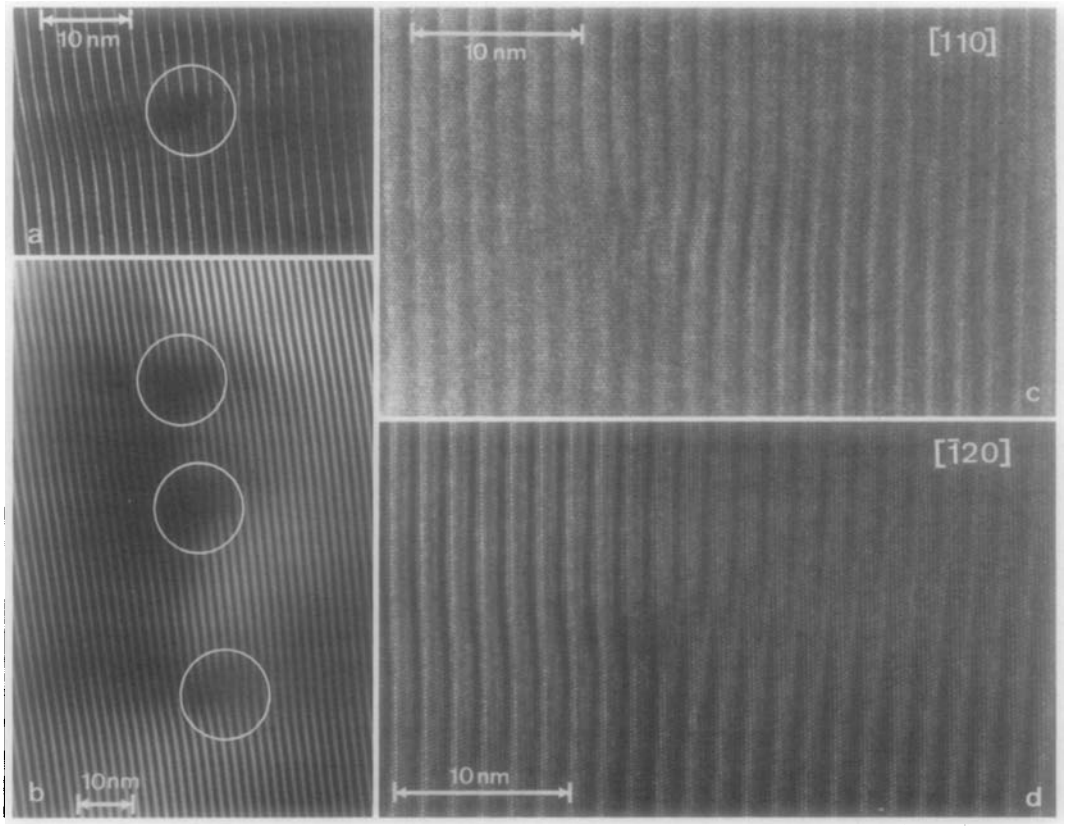

FIG. 21. (a) High-resolution, small magnification image. The bright silicon fringes are prominently visible. One supplementary half fringe is present giving rise to a dislocation-like feature. (b) Moderate-resolution image revealing only the silicon fringes; three "dislocations" are visible in the areas surrounded by circles. (c) High-resolution image of dislocation-like configuration in the silicon fringes as viewed along the [110] zone. (d) Dislocation-like configuration viewed along the [$\bar{1}$20] zone. Note that in both cases the manganese lattice is continuous, i.e., dislocation-free. This can best be observed by looking at grazing incidence along the lattice rows (of dots).

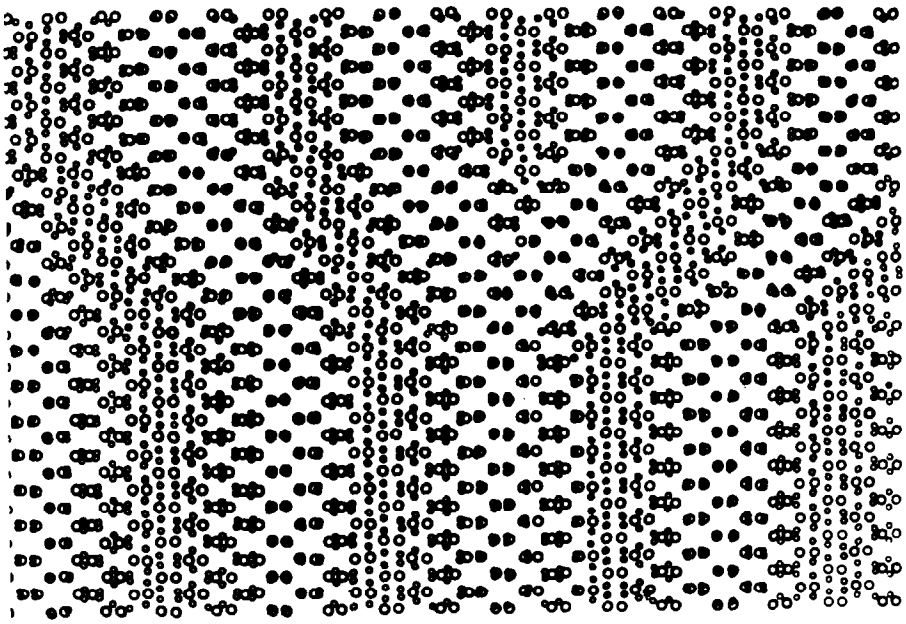

FIG. 22. Atomic model for the dislocation-like configurations observed in $MnSi_{2-x}$. The configuration results from the introduction of a supplementary half row of silicon atoms in the top "half," followed by small shifts of the silicon helices in an undeformed manganese sublattice.

In the core of the "dislocation," magnified in Fig. 23c, the manganese columns are well resolved; it is clear that the manganese sublattice exhibits *no* evidence for the occurrence of a dislocation.

The silicon fringes enclose an angle ϕ with the manganese rows which varies somewhat between 3–5° (Fig. 23d). The area exhibits moreover a crossed grid of moiré-like fringes; one set has a spacing which is the double of that of the other set. The directions and spacings are indicated by white lines on the photograph. The moiré-like fringes with the smallest spacing enclose an angle θ of about 23–26° with the manganese rows. The angular multiplication is in this case $q/\varepsilon = 7$. These three values are clearly consistent with the relation (3) since tg 4° = 0.0699 and tg 26° = 0.489. The direction of the set of broad fringes is not well defined; it is roughly perpendicular to the manganese rows.

The different relevant wave vectors are represented graphically in Fig. 24. The silicon fringes are perpendicular to OP (or RT) and their spacing is 3.5 times the manganese spacing. The narrowly spaced moiré-like fringes have the wave vector $\overline{\Delta}\bar{g}_1 = PS$ which is approximately equal to $1/c_{Si}$; it is twice as long as the wave vector of the widely spaced moiré-like fringes $\overline{\Delta}\bar{g}_3 = PR$ or SQ, which is perpendicular to the normal OT to the manganese fringes. The geometry of the wave vectors of the different types of fringes is thus fully consistent with the composition determined from the high-resolution image.

The fact that there are only two visible sets of moiré fringes is a consequence of the decrease in intensity with increasing order of the satellite reflections. Whereas $\overline{\Delta}\bar{g}_1$ results from the interference between two third-order reflections, $\overline{\Delta}\bar{g}_3$ results from the interference between a third- and a fourth-order reflection. The wave vector RQ resulting from two fourth-order reflections

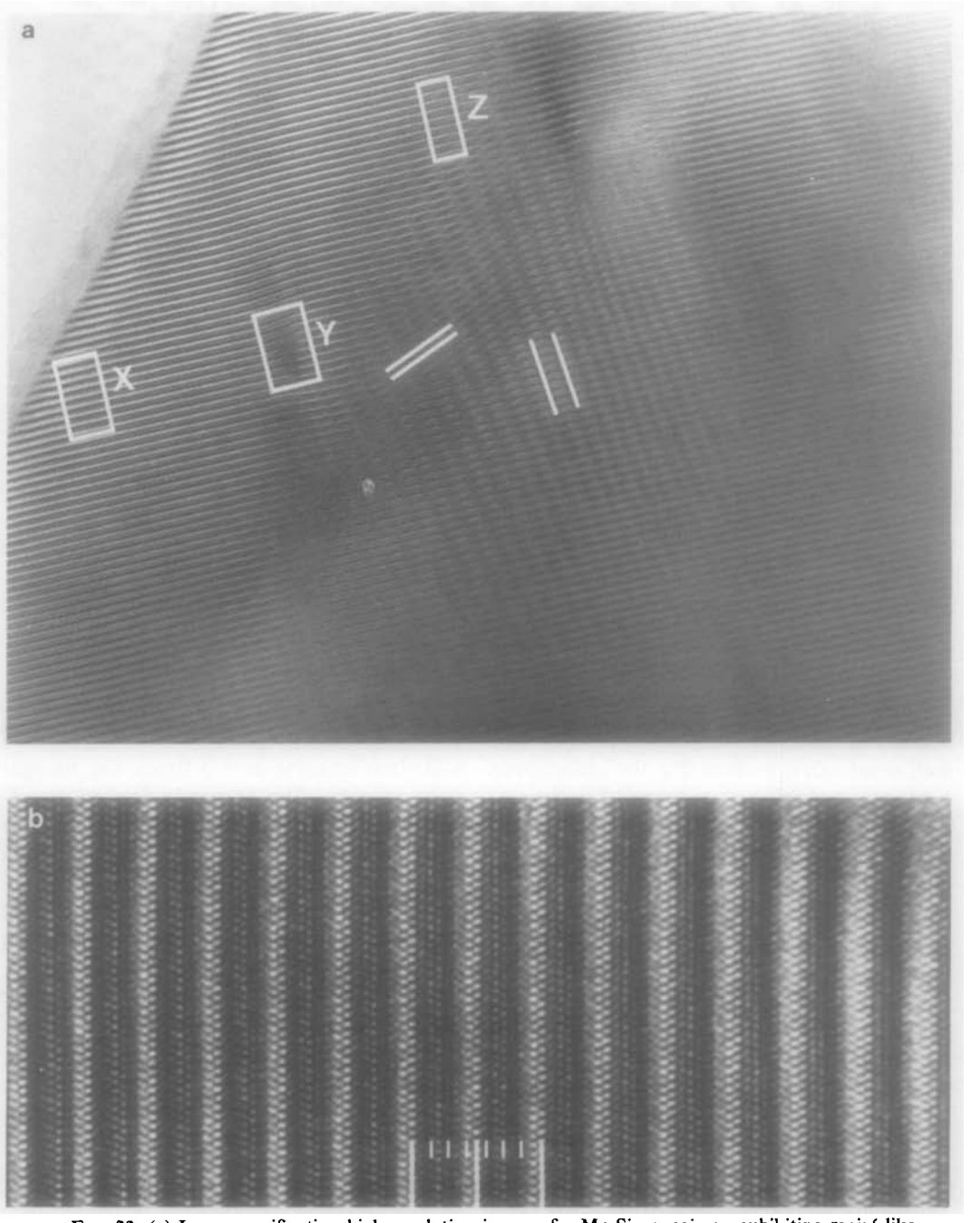

FIG. 23. (a) Low-magnification high-resolution image of a Mn_7Si_{12} specimen exhibiting moiré-like fringes and a dislocation-like configuration. The boxed areas X, Y, and Z are magnified in (b), (c), and (d). (b) High-magnification of the area X; the high-resolution image allows us to identify the compound as Mn_7Si_{12}. (c) High-magnification of the area Y showing the manganese sublattice in the core of the dislocation. (d) High-magnification of the area Z showing the orientation difference ϕ between the manganese and the silicon fringes.

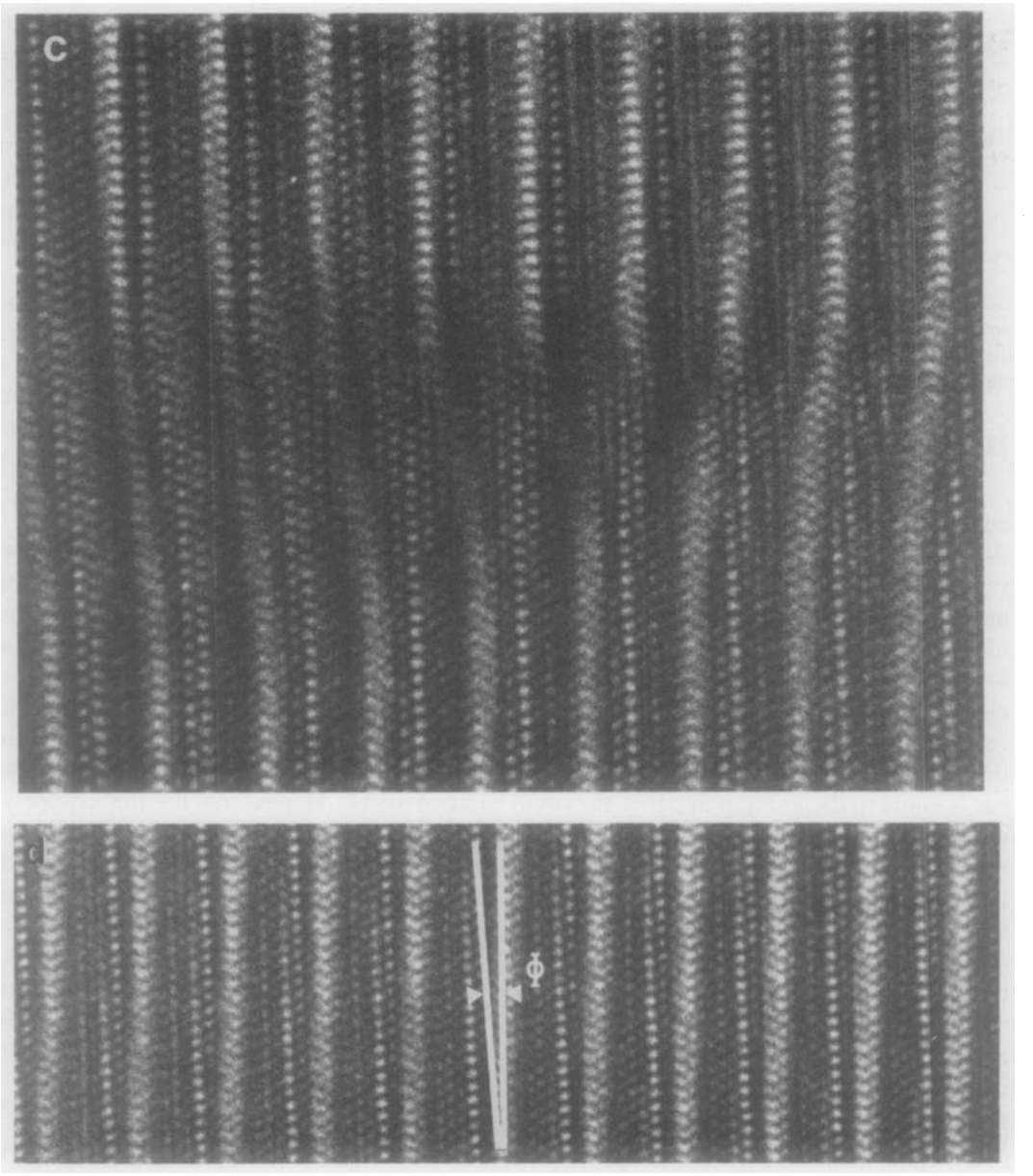

FIG. 23—*Continued.*

leads apparently to fringes which are too weak to be observed against the background of a high-resolution image.

In a compound with this composition the mode 1 (Fig. 19) moiré-like fringes have a spacing $\Delta = c_{Si}$, whenever there is no spacing anomaly (from (*8*)). As a result *no* moiré-like fringes are visible near the edge of the specimen where they coincide with the silicon fringes, which are themselves parallel with the manganese rows there (see Fig. 23).

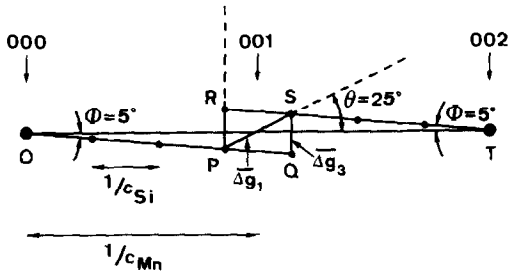

FIG. 24. Schematic representation of the different wave vectors which operate in Fig. 23. Note that the geometry of these wave vectors is fully consistent with the observations of Fig. 23.

11. Phase Stability

Jeitschko and Parthé (*8*) formulated the condition for the stability of compounds of the type TM_2. All such phases of a given type should have the same value for the number of valence atoms per transition metal atom. The transition metal atom is assumed to contribute a number of valence electrons equal to the number of electrons outside the next lower inert gas configuration, i.e., seven for manganese; this number is equal to the group number of the transition element. For silicon the number of valence electrons is four. For compounds of the series Mn_nSi_{2n-m} this constant number is thus $N = [7n + 4(2n - m)]/n = 15 - 4(m/n)$; its constancy implies the constancy of the ratio m/n. For the ideal value 14 this ratio would have to be $m/n = \frac{1}{4}$ and the general formula of these compounds would be $Mn_{4n}Si_{7n}$. The actual data for all compounds observed either in this or in previous work are summarized in Table II; for most of the compounds one has $N = 15 - (4m/4m - 1)$. The rule formulated by Jeitschko and Parthé is thus rather well obeyed especially for large m.

12. Conclusions

The orientation and spacing anomalies observed commonly in electron diffraction patterns of the manganese silicides and of related chimney ladder structures can consistently be explained on the basis of the structure, if a certain form of disorder is allowed for. The disorder consists in a longitudinal shift of the helical arrangements of silicon atoms within the tetragonal manganese sublattice. This model also explains the occurrence of "dislocation-like" configurations in the silicon lattice fringes.

The insertion defects can in a sense be considered as frozen in "phasons." The sliding of the modulation pattern along the c direction within one "chimney" of manganese atoms should be rather easy at high temperature and to some degree only weakly correlated with the sliding in neighboring "chimneys."

In an ideal crystal the modulation patterns in neighboring chimneys would all be correlated, i.e., they would all be in phase and thus form a well-defined commensurate structure, characterized in the electron microscope by the occurrence of straight moiré-like fringes, parallel with the silicon fringes and hence also with the manganese lattice rows. Depending on the composition, the silicon helices may contain silicon vacancies, resulting in a redistribution of the silicon atoms along the chimneys and facilitating the occurrence of phase shifts between the modulation patterns in neighboring chimneys and hence also leading to local structures presenting "anomalies" in the selected area electron diffraction pat-

TABLE II

Compound	n	m	Electrons/T atom = $15 - 4(m/n)$
Mn_4Si_7	4	1	14.00
Mn_7Si_{12}	7	2	13.86
$Mn_{11}Si_{19}$	11	3	13.91
$Mn_{15}Si_{26}$	15	4	13.94
$Mn_{19}Si_{33}$	19	5	13.95
$Mn_{26}Si_{45}$	26	7	13.92
$Mn_{27}Si_{47}$	27	7	13.96
$Mn_{39}Si_{68}$	39	10	13.97

terns. Some parts of the specimens may thus present "incommensurate" areas next to commensurate areas even after long annealing treatments. Since often a continuous transition between the two types of structures is observed in going from one area to another, as deduced from the diffraction pattern and from the moiré-like fringes, it must be concluded that at least in some parts the structure must be incommensurate.

The described sliding of helices may clearly also give rise to the dislocation like defects within a perfect manganese sublattice.

Acknowledgments

We would like to thank Dr. G. Van Tendeloo and Dr. R. De Ridder for the use of unpublished photographs (Figs. 7 and 18).

References

1. H. NOWOTNY, *in* "The Chemistry of Extended Defects in Non-Metallic Solids" (L. Eyring and M. O'Keefe, Eds.), p. 223, North-Holland, Amsterdam (1970); W. B. PEARSON, "The Crystal Chemistry and Physics of Metals and Alloys," p. 594, Wiley–Interscience, New York (1972).
2. R. DE RIDDER, G. VAN TENDELOO, AND S. AMELINCKX, *Phys. Status Solidi A* **33,** 383 (1976); R. DE RIDDER AND S. AMELINCKX, *Mater. Res. Bull.* **6,** 1223 (1971): R. DE RIDDER, J. VAN LANDUYT, AND S. AMELINCKX, *Phys. Status Solidi A* **9,** 551 (1972).
3. H. Q. YE AND S. AMELINCKX, "Modulated Structure Materials" (T. Tsakalakos, Ed.), p. 173, Marinus Nijhoff, Dordrecht (1984).
4. M. H. MULLER AND H. W. KNOTT, Abstract American Cryst. Assoc. Meeting Gatlinburg, Tenn. Paper F2.
5. O. SCHWOMMA, A. PRESINGER, H. NOWOTNY, AND A. WITTMAN, *Monatsh. Chem.* **95,** 1527 (1964).
6. H. W. KNOTT, M. H. MULLER, AND L. HEATON, *Acta Crystallogr.* **23,** 549 (1967).
7. H. NOWOTNY *et al., NBS Spec. Publ. (U.S.)* **364,** 487 (1972); G. H. FLICHER, H. VÖLLENKLE, AND H. NOWOTNY, *Monatsh. Chem.* **98,** 2173 (1967); H. VÖLLENKLE, A. WITTMANN, AND H. NOWOTNY, *Monatsh. Chem.* **97,** 506 (1968).
8. W. JEITSCHKO AND E. PARTHÉ, *Acta Crystallogr.* **22,** 417 (1967).
9. G. VAN TENDELOO AND S. AMELINCKX, *Phys. Status Solidi A* **43,** 553 (1977); **50,** 53 (1978).